Mineralium Deposita (2004) 39: 204–222
DOI 10.1007/s00126-003-0397-5

ARTICLE

Massimo Chiaradia · Lluís Fontboté · Bernardo Beate

Cenozoic continental arc magmatism and associated mineralization in Ecuador

Received: 28 January 2003 / Accepted: 31 August 2003 / Published online: 3 December 2003

Abstract Most of the economic ore deposits of Ecuador are porphyry-Cu and epithermal style gold deposits associated with Tertiary continental arc magmatism. This study presents major and trace element geochemistry, as well as radiogenic isotope (Pb, Sr) signatures, of continental arc magmatic rocks of Ecuador of Eocene to Late Miocene (~50–9 Ma, ELM) and Late Miocene to Recent (~8–0 Ma, LMR) ages. The most primitive ELM and LMR rocks analyzed consistently display similar trace element and isotopic signatures suggesting a common origin, most likely an enriched MORB-type mantle. In contrast, major and trace element geochemistry, as well as radiogenic isotope systematics of the whole sets of ELM and LMR samples, indicate strikingly different evolutions between ELM and LMR rocks. The ELM rocks have consistently low Sr/Y, increasing Rb/Sr, and decreasing Eu/Gd with SiO_2, suggesting an evolution through plagioclase-dominated fractional crystallization at shallow crustal levels (< 20 km). The LMR rocks display features of adakite-type magmas (high Sr/Y, low Yb, low Rb/Sr) and increasing Eu/Gd and Gd/Lu ratios with SiO_2. We explain the adakite-type geochemistry of LMR rocks, rather than by slab melting, by a model in which mantle-derived melts partially melt and assimilate residual garnet-bearing mafic lithologies at deeper levels than those of plagioclase stability (i.e., > 20 km), and most likely at sub-crustal levels (> 40–50 km). The change in geochemical signatures of Tertiary magmatic rocks of Ecuador from the ELM- to the LMR-type coincides chronologically with the transition from a transpressional to a compressional regime that occurred at ~9 Ma and has been attributed by other investigations to the onset of subduction of the aseismic Carnegie ridge.

The major districts of porphyry-Cu and epithermal deposits of Ecuador (which have a small size, << 200 Mt, when compared to their Central Andean counterparts) are spatially and temporally associated with ELM magmatic rocks. No significant porphyry-Cu and epithermal deposits (except the epithermal high-sulfidation mineralization of Quimsacocha) appear to be associated with Late Miocene-Recent (LMR, ~8–0 Ma) magmatic rocks. The apparent "infertility" of LMR magmas seems to be at odds with the association of major porphyry-Cu/epithermal deposits of the Central Andes with magmatic rocks having adakite-type geochemical signatures similar to LMR rocks. The paucity of porphyry-Cu/epithermal deposits associated with LMR rocks might be only apparent and bound to exposure level, or real and bound (among other possibilities) to the lack of development of shallow crustal magmatic chambers since ~9 Ma as a result of a prolonged compressional regime in the Ecuadorian crust. More work is needed to understand the actual metallogenic potential of LMR rocks in Ecuador.

Keywords Porphyry-Cu · Epithermal · Cenozoic Ecuador · Continental arc magmatism

Editorial handling: J. Richards

M. Chiaradia (✉) · L. Fontboté
Section des Sciences de la Terre,
Université de Genève,
Rue des Maraîchers 13,
1205 Geneva, Switzerland
E-mail: m.chiaradia@earth.leeds.ac.uk
Tel.: +44 113 343 5238
Fax: +44 113 343 5259

B. Beate
Departamento de Recursos Minerales y Geoquímica,
Escuela Politécnica Nacional,
AP 17–01–2759, Quito,
Ecuador

Present address: M. Chiaradia
Centre for Geochemical Mass Spectrometry,
School of Earth Sciences,
University of Leeds,
LS2 9JT Leeds, U.K.

Introduction

Precious metal-bearing epithermal and porphyry-Cu deposits result from the interplay of several magmatic, tectonic, and hydrothermal processes occurring at convergent margins (e.g., Sillitoe 2000; Tosdal and Richards 2001). They are associated with shallow level intrusions in the magmatic arc environment (e.g. Sillitoe 2000), and are often located in regions characterized by peculiar styles of crustal deformation and structures (e.g., Corbett and Leach 1998; Tosdal and Richards 2001). Porphyry-Cu and epithermal deposits are genetically associated with arc magmas displaying a broad range of compositions, from low-K calc-alkaline, through high-K calc-alkaline, to alkaline (e.g., Kay et al. 1999; Sillitoe 2000; Tosdal and Richards 2001).

Recently, a preferential association of large Au-bearing porphyry-Cu and epithermal deposits with adakites has been proposed (Thiéblemont et al. 1997; Sajona and Maury 1998; Oyarzun et al. 2001). Adakites are volcanic rocks with geochemical signatures (such as $SiO_2 \geq 56$ wt%, $Al_2O_3 \geq 15$ wt%, $Sr/Y \geq 22$, $Y \leq 18$ ppm, and $Yb \leq 1.8$ ppm), which are thought to indicate slab melting (Defant and Drummond 1990). Because of the supposed origin of adakites, emphasis has been placed on the association of large Au-bearing porphyry-Cu/epithermal deposits with slab melting (Oyarzun et al. 2001; Mungall 2002). However, as pointed out by Garrison and Davidson (2003), the geochemistry of adakites only implies their derivation from a basaltic source in a pressure–temperature field where garnet (±amphibole) is stable and plagioclase is not. The geochemical signatures of adakites, therefore, are not necessarily unique to slab melting and more broadly correspond to high-pressure melting of wet basalt (e.g., Atherton and Petford 1993; Drummond et al. 1996; Garrison and Davidson 2003; see also Castillo et al. 1999 for the interpretation of Philippines adakites). Based on the ground that the rocks with adakitic signatures might derive from processes other than slab melting (like the interaction of mantle-derived magmas with the lower crust), the genetic relationship between slab melts and porphyry-Cu/epithermal mineralization has been questioned (Rabbia et al. 2002; Richards 2002). It has also been suggested that a process of formation of adakite-type rocks (i.e., rocks having geochemical signatures of adakites without evidence of their derivation from slab melting) through interaction of mantle-derived magmas with the lower crust may explain the metallogenic potential of adakite-type rocks of the Central Andes (e.g., Kay et al. 1999; Richards et al. 2001).

In this study we present new geochemical and isotopic data for Tertiary magmatic rocks and Au-bearing porphyry-Cu/epithermal deposits of Ecuador, a region little investigated thus far from this point of view, with the aim to extend the knowledge of the relationships between magma chemistry and porphyry-Cu/epithermal deposits to the Northern Andes. Our data indicate that the large majority of the Tertiary porphyry-Cu and epithermal deposits of Ecuador (e.g., Portovelo-Zaruma, Fierro Urcu, Chaucha, San Gerardo, Gaby, Bella Rica, Tres Chorreras, El Torneado, Peggy, Gañarin, El Mozo) are genetically associated with Eocene to Late Miocene (ELM, ~50–9 Ma) calc-alkaline magmatic rocks that have consistently evolved through AFC (assimilation and fractional crystallization) processes at shallow crustal levels (< 20 km). In contrast, only the ~5 Ma old high sulfidation epithermal deposit of Quimsacocha (Beate et al. 2001) is associated with Late Miocene to Recent (LMR, ~8–0 Ma) magmatic rocks, which are characterized by adakite-like signatures. The apparent low fertility of the adakite-type LMR rocks of Ecuador as compared to the ELM rocks is at odds with the preferential association of large porphyry-Cu/epithermal deposits with adakite-type rocks recognized in the Central Andes (e.g., Kay et al. 1999; Richards et al. 2001; Oyarzun et al. 2001) and in other magmatic arcs (e.g., Philippines: Sajona and Maury 1998), whatever be the origin of these rocks.

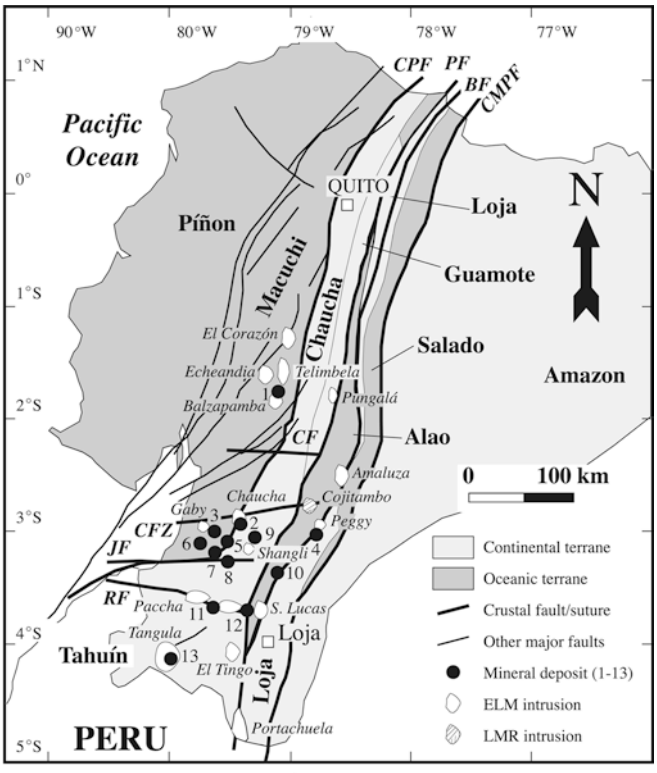

Fig. 1 Geotectonic map of Ecuador (modified after Litherland et al. 1994) showing the locations of some major Tertiary porphyry-Cu and epithermal deposits of Ecuador as well as of some Tertiary intrusions. *CPF* Calacalí-Pallatanga-Palenque fault, *PF* Peltetec suture continuing south into Las Aradas fault, *BF* Baños fault, *CMPF* Cosanga-Mendez-Palanga fault, *CF* Cañar fault zone, *CFZ* Chaucha fault zone, *JF* Jubones fault zone, *RF* Raspas fault zone

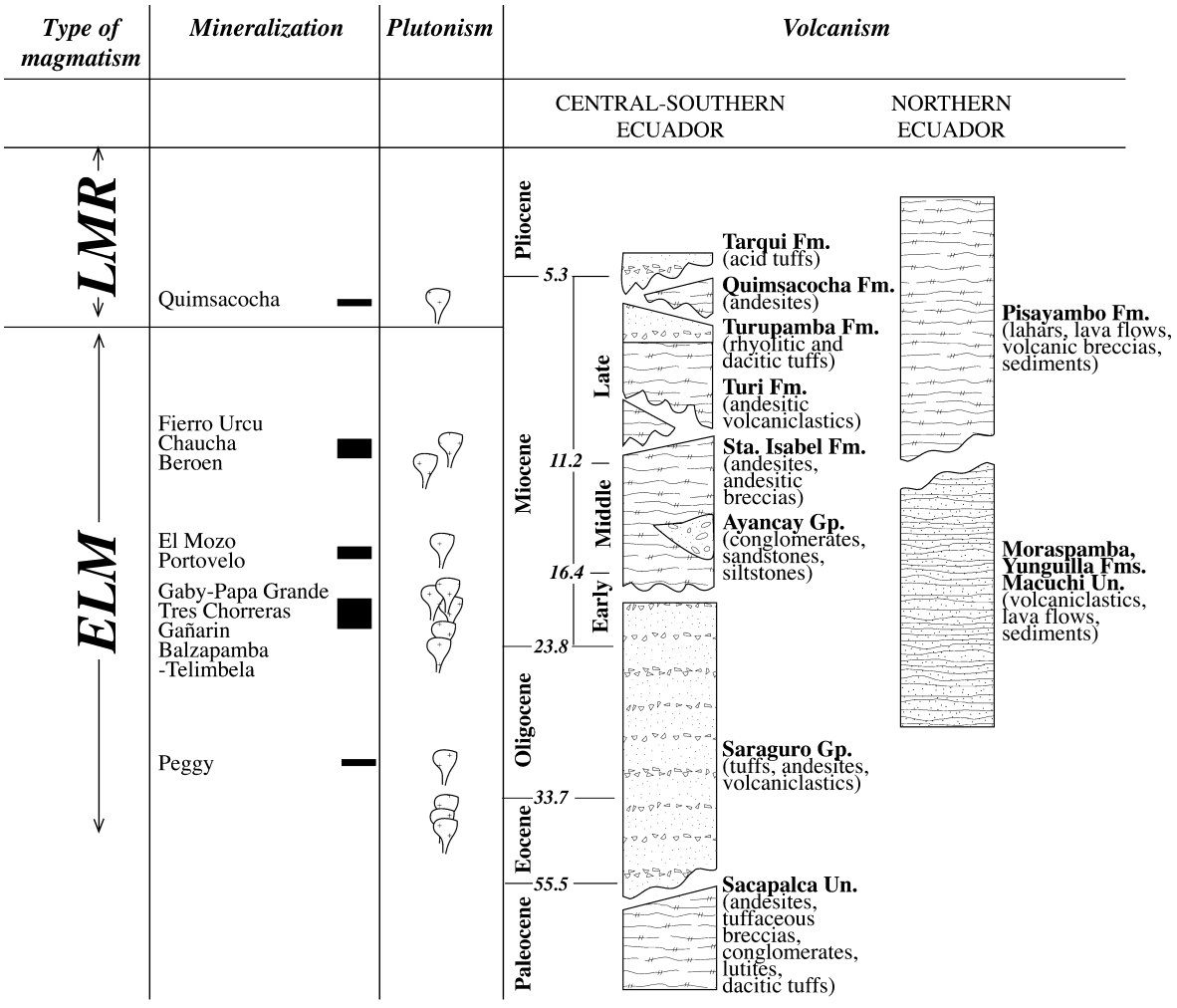

Fig. 2 Stratigraphy of the main lithologic units cropping out in central-southern and northern Ecuador, as well as of the magmatic and ore events (modified from Lavenu et al. 1992, BGS and CODIGEM 1999, and Hungerbühler et al. 2002)

In the present investigation we discuss:

i. The contrasting geochemical features of ELM and LMR rocks
ii. The origin of the adakite-type signatures of LMR rocks
iii. The apparent scarcity of porphyry-Cu/epithermal deposits associated with the LMR rocks
iv. The change of geodynamic regime at the end of the Miocene in Ecuador as possibly responsible for the transition from ELM- to LMR-type magmas.

Geological setting, geodynamic evolution and magmatism

Ecuador consists of several terranes, both with continental and oceanic affinity, which were accreted onto the Amazon craton from the Early Cretaceous to the Eocene (Feininger 1987; Mourier et al. 1988; Aspden and Litherland 1992; van Thournout et al. 1992; Litherland et al. 1994; Jaillard and Soler 1996; Jaillard et al. 1997; Reynaud et al. 1999; Hughes and Pilatasig 2002; Mamberti et al. 2003). From east to west the following domains are recognized (Fig. 1): the Salado marginal basin (Jurassic volcano-sedimentary sequences); the Loja terrane (Paleozoic schists and gneisses, Triassic granites and anatexites); the Alao island arc (Jurassic meta-basalts/andesites); the Guamote, Chaucha and Tahuín terranes (lithologies similar to those of Loja); the Macuchi Early Tertiary island arc (basalts and andesites); the Cretaceous Píñon and Pallatanga oceanic plateaus (basalts and gabbros). Most of these domains are extended for several hundreds of kilometers along a NNE direction and are only few tens of kilometers wide (Fig. 1). The terranes are separated by NNE-trending sutures, which have been continuously reactivated as dextral strike-slip faults (e.g., Aspden and Litherland 1992; Fig. 1). In southwestern Ecuador (south of 2°S), deep crustal E-W/NE-SW strike-slip fault systems and the Raspas suture, separating the Tahuín and Chaucha terranes, mark the transition from the Central to the Northern Andes (Huancabamba deflection; Fig. 1).

The tectonic and magmatic evolution of the Ecuadorian Andes during the Tertiary is controlled by the interplay of various factors, including changing subduction rates, obliquity and angle of subduction, and

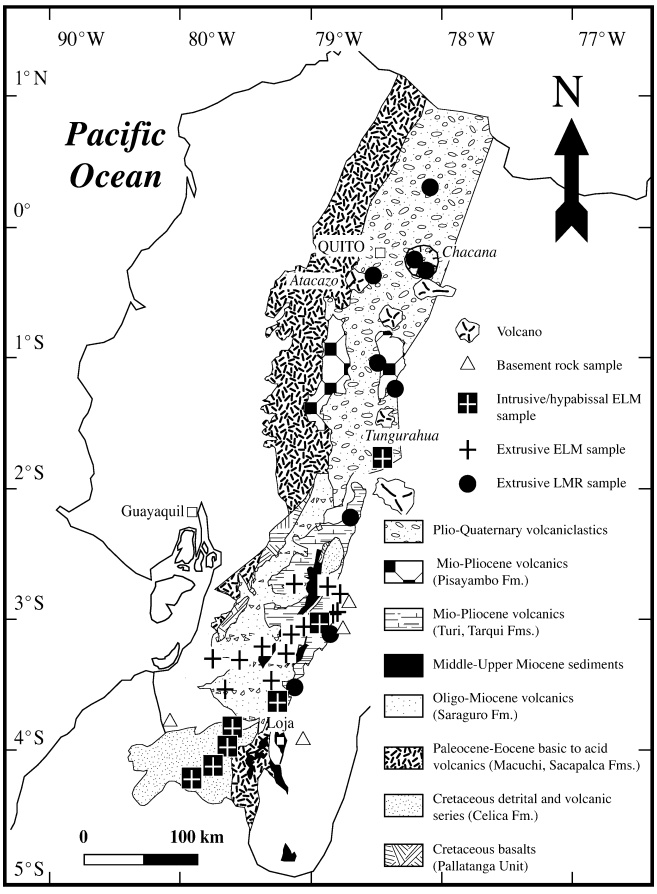

Fig. 3 Simplified geological map of the Tertiary volcanic and volcaniclastic units of cordilleran Ecuador (modified from Lavenu et al. 1992 and Hungerbühler et al. 2002) showing the locations of the samples investigated in the present study

subduction of aseismic ridges (Hungerbühler et al. 2002). Splitting of the Farallon plate into the Nazca and Cocos plates at ~25 Ma forced subduction to become more orthogonal with respect to the trench and more shallow (Hey 1977; Daly 1989). Subduction of the inferred Inca plateau at 10–12 Ma (Gutscher et al. 1999a) and of the Carnegie ridge since 8 Ma (Gutscher et al. 1999b) or perhaps earlier (10–15 Ma: Spikings et al. 2001; Hungerbühler et al. 2002) caused a further shallowing of the subduction zone. The subduction of the inferred Inca plateau south of 2°S might have been responsible for the gradual cessation of volcanic activity in southern Ecuador during the Miocene (e.g., Gutscher et al. 1999a).

The Northern Andes have been subjected mostly to a transpressional regime from Late Oligocene to Miocene (27–5 Ma: Noblet et al. 1996). A period of extension in the Inter-Andean area during the Middle Miocene has been related to removal of crustal support in the Inter-Andean region via a NNE-directed displacement of the coastal Píñon-Macuchi-Pallatanga terranes (Hungerbühler et al. 2002).

At least from the Pliocene until Recent (5–0 Ma) the Northern Andes have been mainly characterized by a compressional regime (Noblet et al. 1996). Steinmann et al. (1999) have identified major Tertiary compressional phases in southern Ecuador between 9 and 6 Ma and from 3 Ma to Recent. Spikings et al. (2001) and Hungerbühler et al. (2002) attribute the compression phase started 9 Ma ago (Steinmann et al. 1997) in the forearc area and in the Inter-Andean region to the Carnegie ridge collision with the Ecuadorian margin.

The Tertiary continental arc magmatic activity in Ecuador is documented by various volcanic formations and intrusions distributed rather continuously throughout time (Fig. 2), although major magmatic pulses seem to have occurred in the Oligocene (35–27 Ma), Miocene (21–8 Ma) and Pliocene (4–2 Ma) (Lavenu et al. 1992). The Paleocene to Early Eocene Sacapalca Unit, which consists of andesitic lavas, tuffaceous breccias, conglomerates, lacustrine lutites and dacitic tuffs, crops out in southwestern Ecuador (BGS and CODIGEM 1999; Figs. 2 and 3). The Oligocene to Early Miocene Saraguro Group crops out extensively in central-southern Ecuador and consists of welded tuffs of dacitic to rhyolitic composition, andesitic to rhyolitic lavas, volcaniclastic material and sediments (BGS and CODIGEM 1999; Figs. 2 and 3). The Miocene Sta. Isabel Formation, which consists of andesitic lavas and tuffaceous breccias (Figs. 2 and 3), is found in central-southern Ecuador. Various Miocene and Pliocene volcanic formations crop out in central-southern Ecuador (Turi, Tarqui, and Quimsacocha Formations: BGS and CODIGEM 1999) and in northern Ecuador (Pisayambo Formation: Lavenu et al. 1992) (Figs. 2 and 3). Available K-Ar (Bristow and Hofstetter 1977; Prodeminca 2000a and 2000b) and fission track datings (Steinmann et al. 1997; Hungerbühler et al. 2002) indicate that abundant plutons were emplaced from the Eocene to the Miocene (Fig. 2) along the Cordillera Occidental (e.g., Balzapamba intrusion, 35–33 Ma; Echeandia intrusion, 26–23 Ma; Telimbela intrusion, 21–19 Ma; El Corazón intrusion, 16–14 Ma; Chaucha batholith, 10–12 Ma), in southwestern Ecuador (e.g., Tangula, ≥48 Ma; El Tingo, 21 Ma; Portachuela, 20 Ma; Paccha, Uzhcurrumi, Shangli intrusions, 20–17 Ma) and in the Cordillera Oriental (e.g., Amaluza, 48 Ma; Pungalá, 42 Ma; San Lucas, ≥39 Ma; Cojitambo, 7.1–5.4 Ma). These plutons are preferentially distributed along the NNE-trending structures and the E-W/NE-SW fault systems of the Huancabamba deflection (Fig. 1), suggesting a structural control on melt emplacement at the regional scale. Litherland and Aspden (1992) have inferred a structural control on present day magma ascent due to the alignment of active volcanic belts of Ecuador with the NNE-trending terrane sutures.

Sampling and analytical methods

Rock sampling

In this study we present geochemical and isotopic data for sixteen Oligocene to Late Miocene volcanic rocks (~30–9 Ma) of the Saraguro Group (N = 7), Sta. Isabel Formation (N = 6) and Turi

Table 1 Major and trace element and isotopic data of the magmatic rocks investigated in this study

Sample	E94004	E94007	E94008	E94021	E94053	E94054	E99003	E99007	E99116	E94020	E94029	E94039	E99004
Lithology	Basalt	Andesite	Andesite	Dacite	Andesite	Andesite	Rhyolite	Dacite	Basaltic andesite	Andesite	Dacite	Andesite	Porphyry rhyolite
Coordinates	0°22'N 78°10'W	0°20'S 78°08'W	0°18'S 78°14'W	3°11'S 78°58'W	1°15'S 78°30'W	0°25'S 78°35'W	2°17'S 78°53'W	3°42'S 79°15'W	1°25'S 78°28'W	3°05'S 78°50'W	3°40'S 79°38'W	2°53'S 78°48'W	3°10'S 79°02'W
Group	LMR	LMR	LMR	LMR	LMR	LMR	LMR	LMR	LMR	ELM	ELM	ELM	ELM
Geologic unit	Pisayambo	Chacana	Chacana	Tarqui	Pisayambo	Atacazo	Tarqui	Tarqui	Tungurahua	Sta. Isabel	Sta. Isabel	Saraguro	Turi
Age	8 Ma[a]	1–3 Ma[b]	1–3 Ma[b]	5 Ma[c]	8 Ma[a]	1 Ma[b]	5 Ma[c]	5 Ma[c]	Recent[b]	15 Ma[c]	15 Ma[c]	25 Ma[a,c]	9 Ma[c]
SiO_2 (wt%)	51.72	56.69	62.03	69.25	56.29	58.20	72.11	66.26	57.36	59.86	63.51	62.88	73.22
TiO_2 (wt%)	0.79	0.92	0.63	0.33	0.90	0.77	0.23	0.48	0.88	0.67	0.49	0.64	0.28
Al_2O_3 (wt%)	15.19	17.71	15.38	17.10	19.14	16.37	15.28	18.16	16.49	17.45	16.37	16.74	14.00
Fe_2O_3 (wt%)	7.99	6.00	4.91	2.08	6.68	7.52	1.92	3.00	7.52	6.30	4.90	5.67	2.45
MnO (wt%)	0.10	0.06	0.08	0.03	0.09	0.10	0.07	0.04	0.12	0.10	0.07	0.09	0.03
MgO (wt%)	9.32	3.96	3.79	0.22	2.72	4.49	0.34	0.29	5.08	3.06	1.43	1.40	0.44
CaO (wt%)	8.20	5.29	5.28	2.62	7.38	7.02	2.16	3.52	6.98	5.99	2.66	4.49	1.89
Na_2O (wt%)	3.54	3.80	3.80	4.57	4.37	3.83	5.01	4.80	3.83	3.55	4.30	4.11	2.82
K_2O (wt%)	0.61	1.89	2.08	1.76	1.19	1.04	1.98	1.49	1.72	1.48	2.77	1.95	3.21
P_2O_5 (wt%)	0.15	0.31	0.26	0.05	0.27	0.18	0.11	0.20	0.24	0.17	0.11	0.30	0.04
LOI (wt%)	1.95	2.66	1.16	1.27	0.80	0	1.01	1.72	0	0.75	2.84	0.84	1.77
Total (wt%)	99.55	99.30	99.38	99.27	99.83	99.27	100.21	99.96	100.20	99.39	99.44	99.12	100.15
Zr (ppm)	63	118	96	113	118	101	123	87	130	102	100	161	159
Y (ppm)	13	10	10	4	13	19	6	5	18	56	12	19	16
Nb (ppm)	4	5	8	4	2	2	11	2	4	2	4	5	9
Rb (ppm)	16	64	65	34	22	18	45	32	45	38	86	55	123
Pb (ppm)	10	13	22	22	15	14	13	10	12	16	15	18	20
Zn (ppm)	74	90	68	68	76	81	77	70	75	78	58	78	45
Cu (ppm)	41	42	26	14	80	38	3	22	47	20	18	18	8
Sr (ppm)	360	1102	657	624	723	546	435	859	596	549	234	438	161
Sc (ppm)	38	23	15	6	12	14	2	3	17	14	11	17	6
Ba (ppm)	354	594	801	928	552	497	891	791	798	558	898	955	1318
V (ppm)	220	170	125	33	174	164	10	68	175	172	94	62	24
U (ppm)	0.4	0.7	2.6	0.7	0.7	< 2*	< 2*	0.8	2*	1.7	1.4	1.8	2.7
Th (ppm)	1.4	3.0	8.1	1.8	2.4	< 2*	3*	2.5	< 2*	4.6	5.7	6.2	12.2
La (ppm)	9.6	25.1	24.9	19.4	16.3	8*	18*	34.5	16*	43.8	16.1	27.3	23.7
Ce (ppm)	19.6	52.2	47.2	35.7	35.6	21*	35*	32.4	36*	98.9	29.0	56.6	43.3
Pr (ppm)	2	4.9	4.0	3.4	3.5			3.7		9.4	2.8	5.2	3.7
Nd (ppm)	10.2	22.5	18.1	15.2	17.1	13*	13*	16.8	21*	47.1	12.3	24.4	15.7
Sm (ppm)	2.7	4.6	3.7	2.7	4.1			3.3		11.0	2.8	5.6	3.5
Eu (ppm)	0.84	1.19	0.91	0.66	1.08			0.79		2.90	0.63	1.37	0.58
Gd (ppm)	3.0	3.7	3.0	1.6	3.8			2.2		11.6	2.7	5.0	3.1
Tb (ppm)	0.5	0.5	0.4	0.2	0.6			0.3		1.7	0.4	0.7	0.5
Dy (ppm)	2.8	2.6	2.4	0.9	3.2			1.3		9.9	2.6	4.4	3.1
Ho (ppm)	0.6	0.44	0.44	0.15	0.61			0.22		2.10	0.53	0.88	0.71
Er (ppm)	1.7	1.2	1.2	0.4	1.7			0.6		6.0	1.5	2.6	2.0
Tm (ppm)	0.2	0.2	0.2	< 0.1	0.3			< 0.1		0.9	0.2	0.4	0.3
Yb (ppm)	1.5	1.0	1.0	0.4	1.5			0.5		5.5	1.5	2.5	2.2
Lu (ppm)	0.22	0.16	0.15	0.05	0.22			0.08		0.80	0.23	0.37	0.33
$^{87}Sr/^{86}Sr$	0.70421 ± 5	0.70476 ± 7	0.70425 ± 6	0.70460 ± 6	0.70408 ± 4			0.70428 ± 6	0.70423 ± 6	0.70418 ± 5	0.70543 ± 6	0.70461 ± 5	0.70604 ± 4
$^{87}Sr/^{86}Sr_i$	0.70420	0.70475	0.70423	0.70459	0.70407			0.70427	0.70422	0.70414	0.70521	0.70448	0.70577
$^{87}Sr/^{86}Sr_r$		0.70463 ± 2						0.70465 ± 6					0.70607 ± 8
$^{206}Pb/^{204}Pb_R$	18.950	18.823	18.902	19.018	18.928			18.882	18.968	18.981	19.000	18.982	19.049
$^{207}Pb/^{204}Pb_R$	15.614	15.613	15.623	15.679	15.607			15.630	15.639	15.661	15.653	15.637	15.645
$^{208}Pb/^{204}Pb_R$	38.673	38.661	38.692	38.878	38.647			38.694	38.761	38.821	38.861	38.749	38.832
$^{206}Pb/^{204}Pb_L$	18.924	18.838	18.894	18.984	18.952			18.867	18.953	18.908	18.991	18.994	19.082
$^{207}Pb/^{204}Pb_L$	15.631	15.633	15.621	15.644	15.648			15.637	15.639	15.624	15.650	15.645	15.662
$^{208}Pb/^{204}Pb_L$	38.713	38.727	38.689	38.772	38.779			38.705	38.739	38.665	38.850	38.804	38.989

Major and trace elements were analyzed by XRF at the CAM (University of Lausanne, Switzerland). REE, U and Th were analyzed by ICP-MS at the X-RAL
Indices of isotope ratios indicate: *i* initial, *R* residue, *L* leachate.*d.l.* detection limit

[a]Lavenu et al. (1992)

[b]Estimated

[c]Hüngerbühler et al. (2002)

[d]Steinmann et al. (1997)

[e]Bristow and Hoffstetter (1977); two K-Ar ages have been obtained on the Tangula batholith, 111 ± 30 Ma (hornblende) and 48 ± 2 Ma (biotite)

[f]Prodeminca (2000a)

[g]corrected at 15 Ma

E99005	E99006	E99009	E99010	E99025	E99026	E99029	E99030	E99046	E99057	E99068	E99069	E99076	E99089
Porphyry rhyolite	Rhyolite	Granite	Andesite	Rhyolite	Rhyolite	Dacite	Diorite	Tonalite	Dacite	Dacite	Dacite	Granite	Andesite
3°20'S	3°33'S	3°45'S	3°45'S	3°57'S	3°56'S	4°05'S	4°06'S	4°15'S	3°20'S	2°54'S	2°50'S	3°06'S	2°59'S
79°10'W	79°13'W	79°14'W	79°14'W	79°26'W	79°28'W	79°35'W	79°34'W	79°55'W	79°45'W	79°09'W	78°54'W	78°50'W	78°52'W
ELM	ELM	ELM	ELM	ELM	ELM	ELM	ELM	ELM	ELM	ELM	ELM	ELM	ELM
Turi	Saraguro	S. Lucas	Saraguro	Saraguro	Saraguro	Saraguro	El Tingo	Tangula	Sta. Isabel	Turi	Saraguro	Peggy	Sta. Isabel
9 Ma[c]	25 Ma[a,c]	≥39 Ma[d]	25 Ma[a,c]	25 Ma[a,c]	25 Ma[a,c]	25 Ma[a,c]	21.2 Ma[c]	≥48 Ma[d]	15 Ma[c]	9 M [c]	20 Ma[e]	32 Ma[f]	15 Ma[c]
73.67	75.18	74.17	61.89	70.05	71.45	67.88	53.87	63.20	64.03	67.67	65.91	71.50	62.73
0.27	0.18	0.20	1.06	0.34	0.39	0.27	0.70	0.60	0.56	0.53	0.39	0.56	0.64
14.26	13.05	13.40	16.21	15.46	14.62	14.62	18.90	16.15	18.25	15.18	16.12	13.43	14.85
2.08	1.77	1.49	6.03	2.00	2.53	2.38	8.72	6.40	3.99	3.25	4.78	3.67	5.87
0.03	0.04	0.03	0.15	0.03	0.03	0.06	0.18	0.14	0.23	0.06	0.18	0.09	0.17
0.55	0.57	0.51	1.83	0.36	1.33	0.16	3.78	2.42	0.85	0.55	1.01	1.28	2.68
2.39	1.49	1.00	4.10	2.67	2.80	4.05	8.60	5.93	4.54	2.98	3.64	1.93	5.65
3.43	3.10	3.87	4.53	3.33	2.49	4.10	2.84	3.65	4.53	3.00	4.26	2.54	3.52
2.70	3.63	4.04	2.21	2.72	2.93	1.99	0.40	0.67	1.23	3.09	2.13	3.45	0.84
0.06	0.04	0.06	0.40	0.13	0.08	0.07	0.15	0.10	0.14	0.14	0.22	0.15	0.22
0.99	1.31	1.26	1.57	1.85	1.65	2.99	2.15	0.81	1.29	3.61	1.59	1.31	2.94
100.42	100.35	100.03	100.00	98.93	100.30	98.57	100.28	100.07	99.64	100.06	100.23	99.92	100.12
145	116	83	188	133	142	132	57	99	141	210	165	180	117
19	22	11	31	16	13	44	16	30	20	23	19	36	24
8	12	11	10	6	4	5	1	< 1	3	7	5	11	5
101	147	108	60	92	72	61	5	16	45	101	61	160	20
17	24	18	10	16	21	14	11	11	49	12	18	22	16
41	39	24	82	38	34	43	78	54	112	51	77	61	290
9	8	6	5	9	9	8	20	15	19	10	6	17	19
176	139	146	412	256	165	231	378	225	419	193	364	125	376
7	4	3	16	6	12	5	11	13	5	11	11	6	16
1174	1211	1121	797	830	909	911	135	398	759	1254	1248	609	348
26	12	20	78	38	81	42	158	138	90	60	24	63	145
2*	2.9	2.3	1.7	2.4	3.5	2.6	0.1	< 2*	2*	< 2*	1.8	5*	< 2*
8*	14.8	15.2	7.6	9.5	20.1	8.5	0.4	< 2*	< 2*	2*	6.8	10*	< 2*
15*	30.6	19.5	28.9	25	18.1	23.2	4.8	< 4*	10*	27*	27.1	20*	10*
28*	57.1	36.5	61.7	48.9	35.3	36.9	12.0	18*	33*	51*	55.6	53*	35*
	5.2	2.9	5.8	4.1	3.1	3.3	1.4				5.1		
12*	21.8	11.5	27.8	17.8	14.0	14.4	8.3	11*	18*	33*	23.3	25*	18*
	4.7	2.5	6.8	3.6	3.1	4.0	2.6				5.0		
	0.48	0.40	1.59	0.78	0.58	1.35	0.83				1.21		
	4.5	2.4	7.0	3.5	2.9	5.8	3.0				4.4		
	0.8	0.4	1.1	0.6	0.5	1.1	0.6				0.7		
	4.7	2.3	6.8	3.3	2.9	7.3	3.4				4.0		
	1.01	0.49	1.37	0.70	0.63	1.72	0.73				0.81		
	2.8	1.3	3.9	2	1.8	5.2	2.2				2.4		
	0.4	0.2	0.6	0.3	0.3	0.8	0.3				0.4		
	3.0	1.4	3.8	2	1.9	4.9	2.3				2.6		
	0.43	0.21	0.57	0.30	0.30	0.76	0.35				0.41		
	0.70677 ± 6	0.70637 ± 4	0.70485 ± 7	0.70513 ± 8	0.70495 ± 7	0.70488 ± 7	0.70442 ± 1			0.70502 ± 6	0.70462 ± 6		
	0.70569	0.70519	0.70470	0.70476	0.70450	0.70485	0.70441			0.70481	0.70448		
	19.045	18.980	18.962	18.905	18.976	18.988	18.912	18.893		19.060	18.980		
	15.656	15.682	15.639	15.639	15.661	15.626	15.640	15.647		15.652	15.656		
	38.852	38.890	38.806	38.709	38.799	38.708	38.686	38.690		38.860	38.777		
	19.089	19.298	18.966	19.010	18.981	19.038	18.890	18.873		19.028	19.111		
	15.662	15.673	15.666	15.653	15.656	15.669	15.635	15.641		15.664	15.655		
	39.006	39.258	38.869	39.210	38.868	38.879	38.676	38.743		38.854	39.037		

laboratories (Toronto, Canada), except where indicated by * (analyzed by XRF)

Formation (N = 3) as well as for five Eocene to Miocene (~50–20 Ma) intrusions: Tangula (≥48 Ma), Pungalá (42 Ma), San Lucas (≥39 Ma), Peggy (32 Ma), and El Tingo (21 Ma). We will refer to these rocks as ELM in the rest of this article (see Table 1 and Figs. 2 and 3). We also present geochemical and isotopic data for nine Late Miocene to Recent (LMR) volcanic rocks (~8–0 Ma) sampled within the Pisayambo Unit (N = 2) in northern and central Ecuador, the Chacana volcanic center (N = 2) in northern Ecuador, the Tarqui Formation (N = 3) in southern Ecuador and two young volcanic centers, Atacazo (N = 1) and Tungurahua (N = 1), in northern-central Ecuador (see Table 1 and Figs. 2 and 3). The ELM and LMR rock groups not only have different ages (Fig. 2) but also different geographic distributions (Fig. 3). ELM rocks crop out in the southwestern part of the country where the crustal-scale, arc normal E–W trending faults and sutures of the Huancabamba deflection are found (Figs. 1 and 3). The LMR rocks crop out in northern and southeastern Ecuador in a crustal domain characterized by the presence only of NNE-trending sutures and faults (Figs. 1 and 3).

Depending on accessibility and outcrop conditions, samples were collected at widespread geographic locations in order to obtain a spatially representative population. Rocks were collected both within mineral deposit districts (e.g., sample E94029 in the Portovelo-Zaruma district, samples E94020 and E99076 close to the Sig-Sig mine) and at locations set apart from mineralization (see Table 1 and Figs. 1 and 3). Particular care was taken in collecting macroscopically unaltered samples. Surface alteration and alteration along fractures were removed when cutting the rock samples for geochemical analyses.

The ages of several volcanic and all intrusive rocks collected in this study (Table 1) are constrained by previous dating of rocks collected from the same outcrops (Bristow and Hofstetter 1977; Steinmann et al. 1999; Hungerbühler et al. 2002). When ages of the sampled outcrops were not available we have used a representative age of the geologic units to which the samples belong (Table 1). Thus, a 25 Ma age has been attributed to samples collected within undated outcrops of the Saraguro Group (Lavenu et al. 1992; Hungerbühler et al. 2002), an age of 15 Ma to undated samples of the Sta. Isabel Formation (Hungerbühler et al. 2002), an age of 9 Ma to undated samples of the Turi Formation (Hungerbühler et al. 2002), an age of 8 Ma to undated samples of the Pisayambo Formation (Lavenu et al. 1992), and an age of 5 Ma to undated samples of the Tarqui Formation (Hungerbühler et al. 2002).

Four metamorphic rocks (two schists from the Paleozoic Chiguinda Unit in the Loja terrane and two meta-andesites from the Jurassic Alao-Paute Unit in the Alao terrane) were also sampled to provide constraints on the isotopic compositions of crystalline basement rocks (Fig. 3).

Multi-element geochemistry and isotope (Pb, Sr) geochemistry

All the ELM and LMR rock samples, as well as the four metamorphic basement rocks (Fig. 3), have been analyzed for major and trace elements (Table 1). Selected magmatic rocks and all metamorphic rocks have been investigated for Pb (N = 24) and Sr (N = 23) isotopic compositions. Twenty-one magmatic rocks have been analyzed for REE, U and Th concentrations by ICP-MS (Table 1). Sulfide minerals (pyrite, chalcopyrite, galena) from ten of the major Au-bearing deposits of Ecuador (Table 2) have also been analyzed for lead isotope compositions (Table 3).

For lead isotope analyses, ore minerals were dissolved in sealed Teflon beakers at 180 °C with a 1:1 mixture of 7 M HCl and 14 M HNO_3. Lead isotopes of rock samples were measured separately on leachate and residue fractions of powdered rocks using the method of Chiaradia and Fontboté (2003). Differences in isotope compositions between residue and leachate fractions are, with few exceptions, virtually within analytical error (Table 1). Those few samples in which leachate and residue fractions differ more significantly are characterized by leachates more radiogenic than residues (Table 1) as expected by the application of this technique to intermediate-felsic magmatic rocks (Chiaradia and Fontboté 2003). The following discussion will concern only residue fractions, which have petrogenetic significance because in intermediate to felsic magmatic rocks they yield isotope compositions closely approximating the common lead signature (Chiaradia and Fontboté 2003).

Lead was purified through chromatography with AG1-X8 and AG-MP1 resins in a hydrobromic medium or by electrodeposition (galena). Fractions of the purified lead were loaded onto rhenium filaments using the silica gel technique and were analyzed for isotope ratios on a MAT-Finnigan 262 thermal ionization mass spectrometer at the Department of Mineralogy of the University of Geneva (Switzerland). The isotope ratios were corrected for fractionation by a factor of +0.08% per amu, based on 157 analyses of the international standard SRM-981. The 2σ reproducibility was 0.05% for the $^{206}Pb/^{204}Pb$, 0.08% for the $^{207}Pb/^{204}Pb$, and 0.10% for the $^{208}Pb/^{204}Pb$ ratio. Total Pb blank contamination (< 120 pg) was insignificant relative to the amounts of Pb analyzed.

Strontium isotopes were measured on bulk rocks digested in Teflon bombs heated at 180 °C for 1.5 h in a microwave oven. Fractions of three samples previously leached in aqua regia at 180 °C for 24 h yielded results virtually identical to those of the bulk fractions (Table 1). Strontium isotope ratios were also measured on the MAT Finnigan 262 mass spectrometer at the Department of Mineralogy of the University of Geneva (Switzerland). The $^{87}Sr/^{86}Sr$ ratios were mass fractionation corrected to an $^{88}Sr/^{86}Sr$ ratio of 8.375209. The $^{87}Sr/^{86}Sr$ ratios obtained were time-corrected ($^{87}Sr/^{86}Sr_i$) using the ages reported in Table 1. The uncertainties in the age of some samples used for time-corrections do not significantly affect the calculated initial Sr isotope ratios because there is a clear-cut age difference between most ELM and LMR rocks and because of the young ages of the rocks analyzed.

Re-Os dating

One Re-Os dating on a molybdenite sample (E99000) from the El Torneado porphyry Cu-Mo deposit was carried out at the laboratory of the Isotope Geology Group of the University of Bern (Switzerland). About 1 mg of pure molybdenite, handpicked from a molybdenite vein hosted by the porphyry intrusion, was weighed together with a ^{185}Re spike and an ICP standard Os solution from Johnson & Matthey in a Carius tube. After sealing the Carius tube, the molybdenite was digested and homogenized with the Re spike and Os standard solution in inverse aqua regia (HNO_3:HCl = 2:1) at 220 °C for 3 days. During weighing and welding the Carius tube was held at −25 °C to avoid evaporative loss of osmium (Schoenberg et al. 2000). Osmium was distilled into HBr using the technique of Nägler and Frei (1997) and purified by microdistillation (Roy-Barman and Allègre 1995). After drying, the Os was ready for measurement. Rhenium was separated from the residual solution of the first Os distillation step by solvent extraction (Walker 1988).

Rhenium and osmium isotope compositions and concentrations were measured on a 12-collector NU Instruments MC-ICP-MS at the University of Bern (Switzerland). In-run fractionation correction of the $^{185}Re/^{187}Re$ ratio was achieved by measuring the known $^{191}Ir/^{193}Ir$ ratio of an Ir standard solution added to the sample. Rhenium was measured in time-resolved mode in order to limit memory effects.

The stable $^{192}Os/^{188}Os$ ratio was used for internal fractionation correction of osmium isotope ratios. Isotopes of elements (^{186}W, ^{187}Re, ^{190}Pt, ^{192}Pt) that potentially interfere with Os isotopes were monitored by measuring ^{182}W, ^{185}Re, and ^{194}Pt. Total procedure blanks were < 20 pg for Re and < 1 pg for Os. Results are reported in Table 4.

The analysis of a ~1 mg aliquot of molybdenite powder from the HLP-5 sample (Huanglonpu carbonatite-hosted deposit, China), carried out as an inter-laboratory check on our results, yielded a 221.9 ± 1.1 Ma age which is in agreement with the 221.3 ± 0.24 Ma age reported by Markey et al. (1998).

Table 2 Summary of geological information on selected Tertiary porphyry-Cu and epithermal deposits of Ecuador

Porphyry-Cu and Au-bearing epithermal deposits of Ecuador

Deposit	Type	Location	Age (Ma)	Reserves	Host Unit	Associated intrusions	Reference
Portovelo-Zaruma	Epithermal IS Au-Ag (Cu-Zn-Pb)	79°37'W, 3°44'S	15–16 (K-Ar)	9.1 Mt @ 13.3 g/t Au, 62 g/t Ag, 0.9% Cu, 1% Zn (extracted)	Andesite porphyry stocks in a thick silicified andesitic volcaniclastic sequence	El Poglio dioritic porphyries	Spencer et al. (2002); Prodeminca (2000b)
				120000 t @1% Cu, 1.7% Zn, 63 g/t Ag, 12 g/t Au (reserves in 1992)			Van Thournout et al. (1996)
Fierro Urcu	Epithermal HS Cu-Au-Ag	79°20'W, 3°45'S	9.6? (K-Ar)	53.5 Mt @ 0.2% Cu and 0.3 g/t Au	Andesites (Sacapalca Fm.)	Porphyritic granodiorites and microdiorites	Prodeminca (2000b)
Chaucha	Porphyry Cu-Mo ± Au	79°25'W, 2°57'S	10–12 (K-Ar)	55 Mt @ 0.57% Cu and 0.3% Mo	Chaucha quartz-hornblende porphyry granodiorite	Chaucha quartz-hornblende porphyry granodiorite	Prodeminca (2000b); Goossens and Hollister (1973)
Gaby-Papa Grande	Porphyry Cu-Au	79°42'W, 3°06'S	19.3 (K-Ar)	165 Mt @ 0.73 g/t Au, 0.12% Cu	Porphyry tonalite to diorite	Porphyry tonalite to diorite	Prodeminca (2000b)
Balzapamba-Telimbela	Porphyry Cu-Mo-Au-Ag	79°12'W, 1°40'S	25.7, 21.4–19.4, 10.8 (K-Ar), 19.9 (Re-Os)	0.71–1.38% Cu (tonnage not measured)	Porphyry granodiorite	Porphyry granodiorite	Prodeminca (2000b); Kennerley (1980); this study
Tres Chorreras-Guabisay-Gigantones-La Tigrera-La Playa	Epithermal Au and Porphyry Cu-Au-Mo	79°23'W, 3°12'S	18–20? (K-Ar)	5.26 Mt @ 3.4 g/t Au (La Tigrera)	Dacite—rhyolitic ignimbrite (Saraguro Group)	Hornblende granodiorite	Prodeminca (2000b)
Los Linderos	Porphyry Cu	80°06'W, 4°18'S	Pot-Eocene	Not available	Granodiorite porphyry	Granodiorite porphyry	None
Laguar	Epithermal Au	80°02'W, 4°21'S	Post-Eocene	Not available	Granodiorite porphyry	Granodiorite porphyry	None
Peggy	Hydrothermal breccia Cu-Ag-Au	78°47'W, 3°07'S	32 ± 1 (K-Ar)	7.36% Cu, 170 g/t Ag, 0.6 g/t Au (reportedly small volume body)	Chlorite schists (Alao Unit) and Tertiary andesites-dacites	Rhyolitic dykes and stocks (32 ± 1 Ma)	Prodeminca (2000b)
Gañarin	Epithermal LS Au	79°24'W, 3°22'S	21.2 ± 0.8 (K-Ar)	Not available	Rhyolitic ignimbrites (Jubones Fm., Upper Oligocene)	Porphyry andesite (22.8 ± 1 Ma)	Prodeminca (2000a)
Beroen	Epithermal LS Au-Ag	79°26'W, 2°55'S	10–12 (K-Ar)	Not available	Andesites (Saraguro Group)	Diorite (Chaucha batholith?)	Prodeminca (2000a)
El Mozo	Epithermal HS Au	79°03'W, 3°25'S	15.4 ± 0.7 (K-Ar)	Not available	Volcanic and pyroclastic rocks (Saraguro Group)	High level intrusions	Prodeminca (2000a)
Quimsacocha	Epithermal Au ± Ag HS	79°14'W, 3°05'S	5 (Zircon fission tracks)	Not available	Andesites and andesitic breccias	Dacitic porphyries; post-ore dacite and rhyolite crop out at caldera rim	Prodeminca (2000a) Beate et al. (2001)

IS intermediate sulfidation, *HS* high sulfidation, *LS* low sulfidation

Table 3 Representative lead isotope analyses of some Tertiary porphyry-Cu and epithermal deposits of Ecuador

Deposit/District	Mineral	$^{206}Pb/^{204}Pb$	$^{207}Pb/^{204}Pb$	$^{208}Pb/^{204}Pb$
Portovelo-Zaruma	Galena	18.959	15.661	38.852
Chaucha	Pyrite	18.962	15.647	38.738
Gaby-Papa Grande	Chalcopyrite	18.966	15.632	38.733
Balzapamba (El Torneado)	Chalcopyrite	18.579	15.595	38.345
Tres Chorreras-Guabisay-Gigantones-La Tigrera-La Playa	Pyrite	18.959	15.660	38.845
Beroen-Molleturo	Pyrite	18.962	15.647	38.738
Los Linderos	Chalcopyrite	18.758	15.656	38.712
Laguar	Pyrite	18.803	15.646	38.682
Peggy	Pyrite	18.828	15.669	38.842
Gañarin	Pyrite	18.715	15.645	38.564
Quimsacocha	Pyrite	18.999	15.657	38.804

Results

Magmatic-related ore deposits

Most of the major Tertiary Cu-Au porphyry and Au epithermal deposits of Ecuador are concentrated in the central-southern part of the country and are preferentially located in proximity to terrane sutures and crustal faults where continental arc ELM intrusive rocks were also emplaced (Fig. 1). This observation suggests that major crustal structures play an important role on the formation of porphyry-Cu/epithermal deposits of Ecuador similarly to other porphyry-Cu/epithermal districts (e.g., Corbett and Leach 1998; Tosdal and Richards 2001). Deposits in central and southern Ecuador include Portovelo-Zaruma, Fierro Urcu, Chaucha, San Gerardo, Gaby, Bella Rica, Tres Chorreras, Gigantones, La Tigrera, La Playa, Quimsacohca, El Torneado, Peggy, Los Linderos, Laguar, Gañarin, and El Mozo (e.g., Prodeminca 2000a and 2000b: the location of the deposits is reported in Fig. 1). Many of them have been/are mined for Au and Ag. The available literature on the geology of these deposits is scant. Descriptions can be found in Goossens (1972), Goossens and Hollister (1973), van Thournout et al. (1996), Prodeminca (2000a and 2000b), and Spencer et al. (2002). The essential geological information given below and in Table 2 is drawn from these sources and from our own field observations. It is worth noting that all these deposits, having tonnages lower or, in most cases, much lower than 200 Mt (Table 2), are significantly smaller than the giant magmatic-related deposits of the Central Andes.

Peggy is a polymetallic (Cu, As, Bi, Sn, W, Pb) breccia pipe associated with small intrusions and dykes of an intensely altered mid-Oligocene (32 Ma?) rhyolite-porphyry at the intersection between the regional NNE-trending Baños Shear Zone and WNW-trending fractures.

The low-sulfidation Au epithermal deposit of *Gañarin* comprises a system of structurally-controlled steep veins with locally high grades of Au and Ag. A K-Ar dating of adularia gives a 21 Ma age for the mineralization (Prodeminca 2000a), which is probably related to the development of a caldera and associated intrusions.

Table 4 Molybdenite Re-Os dates of sample E99000 (El Torneado porphyry, Ecuador) and of the inter-laboratory standard HLP-5 (Huanglonpu carbonatite-hosted deposit, China) which has an age of 221.3 ± 0.24 Ma (Markey et al., 1998)

Sample	Sample weight (g)	Re (ppm)	^{187}Os (ppb)	Re-Os age (Ma)
E99000	0.00134	488.4	101.0	19.7 ± 0.3
HLP-5	0.00128	255.1	607.1	221.9 ± 1.1

The *El Torneado* porphyry-Cu (Balzapamba district, central-southern Ecuador) consists of a disseminated ore (pyrite > chalcopyrite) cut by NNE-trending stockwork-vein ore zones (pyrite, chalcopyrite, molybdenite, magnetite, scheelite, pyrrhotite). El Torneado and other similar deposits of the Balzapamba district are hosted by granodiorites with ages ranging from 34 to 20 Ma (Prodeminca 2000b). The Re-Os dating of molybdenite of the El Torneado porphyry-Cu (sample E99000, Table 4) performed in the present study yielded an age of 19.9 ± 0.3 Ma.

The Cu-Au ± Mo breccia-porphyry system of *Gaby-Papa Grande* is related to porphyritic intrusions dated at 19.3 Ma (Prodeminca 2000b). The main ore stage post-dates the breccia and the highest gold grades are controlled by rock permeability, being found in the magmatic and hydrothermal breccias.

The *Ponce Enriquez* district (including the *Bella Rica, San Gerardo*, and *Muyuyacu* deposits) is hosted by Early to Mid-Cretaceous basalts, gabbros and serpentinites of the Pallatanga Unit intruded by quartz-diorite and microtonalite porphyries of Miocene age (e.g., 19 Ma old Gaby, Tama, Papa Grande porphyries). The mineralization (pyrrhotite, pyrite, arsenopyrite, chalopyrite, with minor amounts of sphalerite, galena, hematite, and traces of molybdenite, sulfosalts, and rare native gold) is found in hydrothermal and magmatic breccias related to the Miocene porphyries and in NNW-trending vein systems. In *Bella Rica*, two mineralized vein systems (pyrite, pyrrhotite, chalcopyrite, marcasite, hematite, gold, ± arsenopyrite ± sphalerite ± tetrahedrite) are associated with small bodies of fine-grained quartz-diorite.

The *Portovelo-Zaruma* mine district is one of the most important active districts of Ecuador with a historic gold production exceeding 4.5 Moz. The gold is

hosted by vein systems developed in the footwall of thrusts within competent host volcanic rocks (Spencer et al. 2002). The vein systems are associated with porphyry intrusions, one of which has been dated at 16 Ma (Pratt et al. 1997). The mineralization is classified as intermediate sulfidation epithermal (Spencer et al. 2002).

The 10–12 Ma old calc-alkaline Chaucha batholith (tonalite-microdiorite-dacite) hosts the porphyry-Cu deposit of *Chaucha*, which has a barren potassic core, a Cu-Mo phyllic zone, an inner pyrite-rich propylitic subzone, and a peripheral propylitic zone. The porphyry-Cu deposit location appears to be strongly controlled by the intersection of two major crustal structures, the NNE-trending Cordillera fault and the E–W Chaucha fault (Goossens and Hollister 1973).

The low sulfidation Au-Ag deposit of *Beroen* (*Molleturo* district), hosted by extensively altered andesitic volcanic rocks of the Saraguro Group, is related to high-level dioritic intrusions probably associated with the 10–12 Ma old Chaucha batholith, exposed in the lower part of the system.

The Cu-Mo porphyry of *Los Linderos* is emplaced within andesites and basaltic andesites of the Cretaceous Celica Formation. The ore consists mostly of malachite with traces of gold and silver.

In *Laguar*, a vein system, carrying Cu, Au, Ag, and Pt cuts the granodiorites of the Late Cretaceous-Early Tertiary Tangula batholith. The mineralization, consisting of pyrite, hematite, chalcopyrite, and gold, is related to a quartz-porphyry.

The high-sulfidation gold mineralization of *Quimsacocha* was emplaced in faults, fractures, diatremes, and breccia bodies of tectonic and hydrothermal origin related to the late Miocene (~5 Ma) development of a caldera (Beate et al. 2001).

In summary, Tertiary porphyry-Cu and epithermal deposits of Ecuador were formed between 5 and 30 Ma, with the majority of the deposits being formed between 20 and 10 Ma (Table 2; Fig. 2). Apart from the Quimsacocha high sulfidation epithermal field, which is associated with the Late Miocene to Pliocene (~5 Ma) adakite (LMR)-type rocks (Beate et al. 2001), all other deposits are both geographically and chronologically related with ELM magmatism (Figs. 1, 2, and 3; Table 2).

Lead isotope compositions of most Oligo-Miocene deposits of Ecuador (Table 3) fall within the compositional field of the Tertiary magmatic rocks suggesting a largely magmatic origin of the lead in the mineralization (Fig. 4). Only El Torneado has a slightly less radiogenic isotopic composition (Fig. 4).

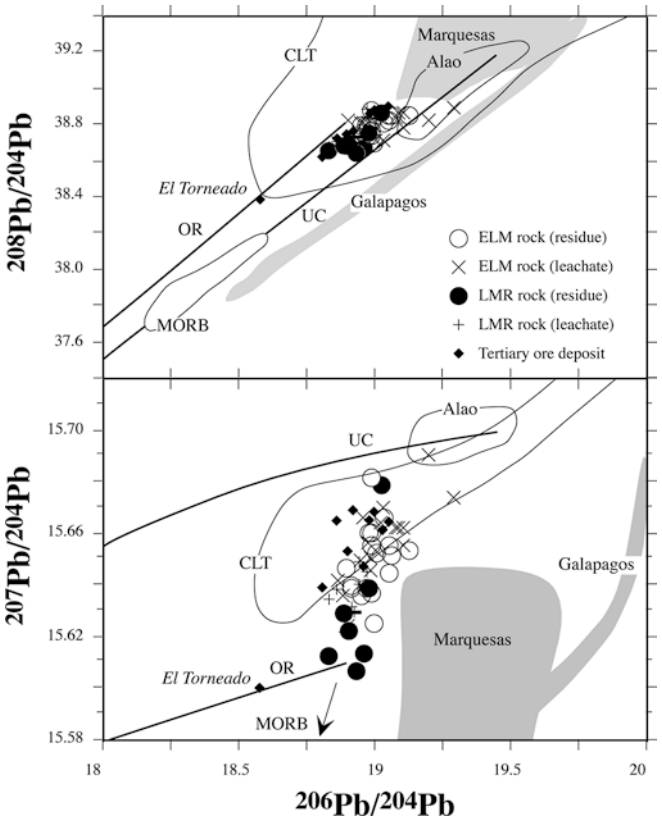

Fig. 4 Lead isotope compositions of leachate and residue fractions of magmatic rocks investigated in this study. The fields of the Chaucha-Loja-Tahuín (*CLT*) and Alao terranes are from this study, Chiaradia and Fontboté (1999), and Chiaradia et al. (submitted 2003). The fields of the Marquesas and Galapagos rocks are from Zindler and Hart (1986). The upper crust (*UC*) and orogen (*OR*) evolution curves are from Zartman and Doe (1981)

Petrography, geochemistry and isotopic compositions of the ELM magmatic rocks

The investigated ELM rocks span a relatively large time interval between ~50 and 9 Ma, although 10 of the 16 ELM volcanic rocks are younger than 20 Ma and only four samples (all intrusive rocks) are older than 30 Ma (Table 1). The ELM volcanic rocks are porphyritic and consist of plagioclase, clino- and orthopyroxene ± K-feldspar phenocyrsts in a matrix of plagioclase, pyroxene, minor amphibole and glass. Apatite is the main accessory mineral. The plagioclase phenocrysts are optically zoned and generally idiomorphic, although sometimes they may have sinuous rims. Intrusive (sample E99009) and hypabyssal (sample E99091) rocks of the ELM group are characterized by the additional presence of biotite. The microscopic analyses of thin sections of the studied samples only in some cases (samples E99010 and E99090) have revealed a partial replacement of amphibole, pyroxene and biotite by chlorite.

The ELM rocks range in composition from calc-alkaline basaltic andesite to rhyolite in the TAS classification diagram (LeBas et al. 1986: Fig. 5). Primitive mantle-normalized spectra of these rocks show subduction-related features, i.e., LILE-enrichment (Ba, Rb, K, Sr) and HFSE (Nb, Ti) depletion (e.g., Pearce 1983; Fig. 6). This suggests derivation of the parent magmas of these rocks from a mantle wedge fluxed by subduction-related fluids carrying LILE elements (e.g., Pearce

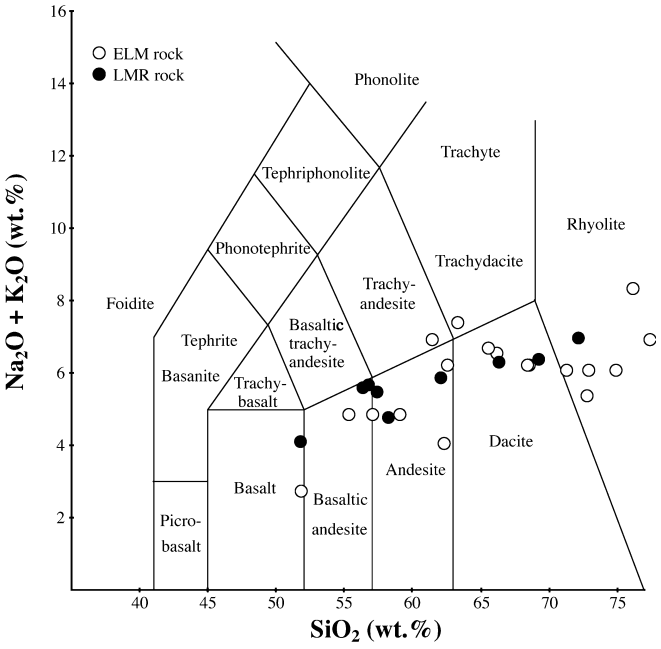

Fig. 5 Geochemical classification of the investigated rocks after LeBas et al. (1986)

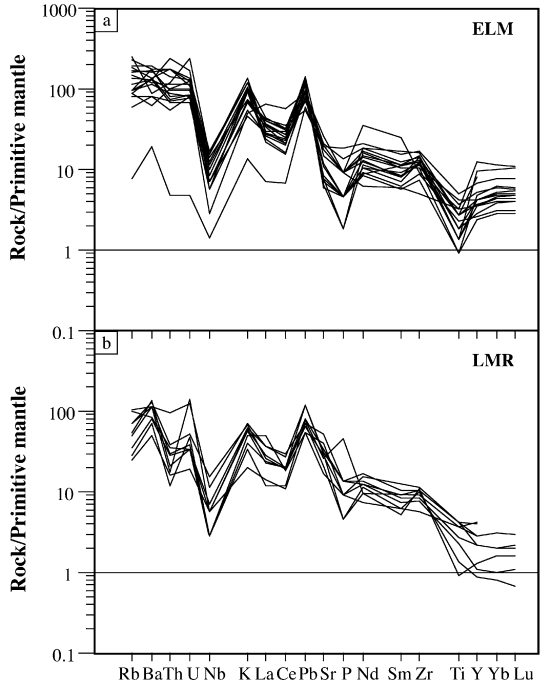

Fig. 6 Primitive mantle-normalized spider diagrams of ELM and LMR rocks investigated in this study (normalization values are from Sun and McDonough 1989)

1983). Major and trace elements of ELM rocks display correlated trends (Fig. 7), such as steady decreases of Al_2O_3, Sr, and increasing Rb/Sr with SiO_2 (Fig. 7). They also display variable LREE fractionation (La/Lu = 10–118; La/Gd = 2–7), almost flat MREE to HREE profiles (Gd/Lu = 8–12, Figs. 8 and 9), variably negative Eu anomalies (Fig. 8), and a systematic decrease of Eu/Gd (a ratio that we use as a proxy of plagioclase fractionation) with SiO_2 (Fig. 9).

Lead isotope compositions of the residual fractions of ELM magmatic rocks ($^{206}Pb/^{204}Pb = 18.8–19.1$; $^{207}Pb/^{204}Pb = 15.62–15.68$; $^{208}Pb/^{204}Pb = 38.6–38.9$) plot between the orogen and upper crust evolution curves in conventional isotope diagrams (Fig. 4). The initial $^{87}Sr/^{86}Sr$ compositions of the ELM rocks range between 0.7041 and 0.7058. The Sr (and to a less extent the Pb) isotope ratios of ELM rocks are fairly well correlated with SiO_2, CaO and Eu/Gd (Figs. 10 and 11).

Petrography, geochemistry and isotopic compositions of the LMR magmatic rocks

The investigated LMR (~8–0 Ma) volcanic and subvolcanic rocks display porphyritic textures and a mineralogical composition similar to the ELM rocks, but are characterized by a more ubiquitous presence of biotite and amphibole phenocrysts. Plagioclase phenocrysts are zoned and often consist of a core with sinuous rims subsequently overgrown by idiomorphic plagioclase. Apatite is the main accessory mineral.

The LMR rocks studied range from calc-alkaline basalt to rhyolite similar to the ELM rocks (Fig. 5). Primitive mantle-normalized spectra show that, like ELM rocks, the LMR rocks also have a typical subduction-related signature (i.e., LILE-enrichment and Th, Nb, Ti depletions; Fig. 6). However, in contrast with ELM magmatic rocks, LMR magmas display no systematic decrease in Al_2O_3 and Sr with SiO_2 (Fig. 7), and are characterized by moderate increases in Na_2O and K_2O and by consistently low Rb/Sr with increasing SiO_2 (Fig. 7). They do not show marked negative Eu anomalies (Fig. 8), and are characterized by positive correlations of Eu/Gd and Gd/Lu with SiO_2 (Fig. 9). LMR rocks also display variably depleted MREE to HREE profiles when compared to ELM rocks (Fig. 8).

Although LMR rocks have lead isotope compositions ($^{206}Pb/^{204}Pb = 18.8–19.0$; $^{207}Pb/^{204}Pb = 15.60–15.68$; $^{208}Pb/^{204}Pb = 38.7–38.9$) generally less radiogenic than those of ELM rocks, they overlap the same compositional field of ELM rocks in conventional isotope plots (Fig. 4). The Sr isotope compositional range of the LMR rocks is narrower and less radiogenic than that of ELM rocks (0.7040–0.7047: Fig. 10). In the isotope ratio versus SiO_2 and CaO plots, LMR rocks plot on the same array of ELM rocks (Fig. 10). In contrast, in the isotope ratio versus Eu/Gd and Gd/Lu diagrams (Fig. 11) LMR rocks define different arrays as compared to those of ELM rocks.

Discussion

The ELM and LMR rocks define trends that converge towards a common least evolved and least radiogenic end-member in the REE versus SiO_2 and REE versus

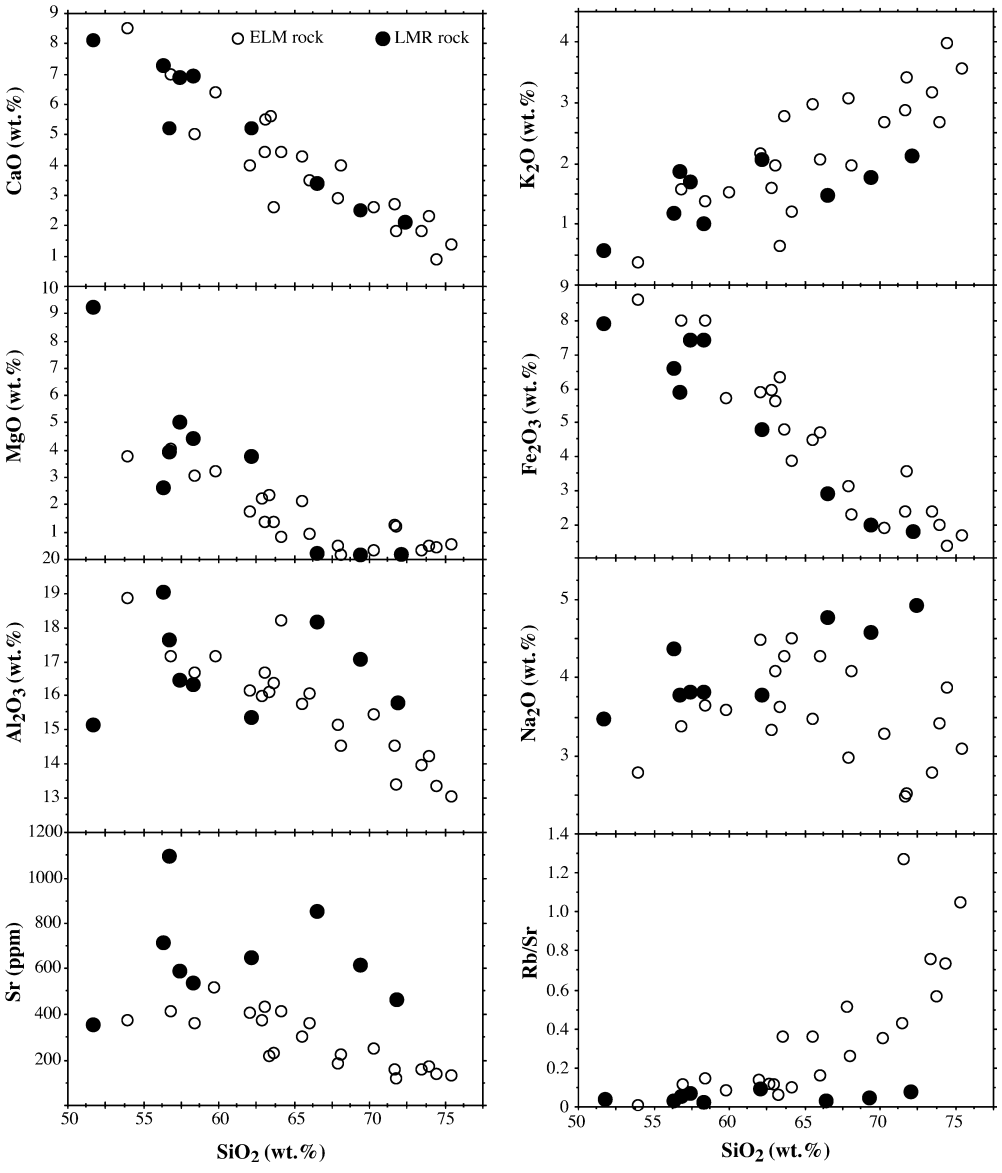

Fig. 7 Major and trace element covariation plots of the magmatic rocks investigated in this study

isotope ratios, as well as in the Pb isotope spaces (Figs. 4, 9, 10, 11, and Table 1). Trace elements (Fig. 6) are compatible with such a common end-member being a basic magma derived from a MORB-type mantle enriched by subducting slab fluids, in agreement with conclusions of previous studies on Andean magmatism (Francis et al. 1977; Hawkesworth et al. 1979; Harmon et al. 1981; Barreiro and Clark 1984; Chiaradia and Fontboté 2002). The most primitive, basaltic rocks of both groups (E99030 for ELM and E94004 for LMR) have relatively radiogenic $^{207}Pb/^{204}Pb$ ratios (>15.61) indicating their derivation from a mantle source enriched by pelagic-sediment lead, like the Early Tertiary mantle of Ecuador (Chiaradia and Fontboté 2001).

The correlated trends of the ELM rocks in the geochemical and isotopic spaces (Figs. 7, 9, 10 and 11) indicate that, despite the different ages (~50–9 Ma), the ELM rocks were formed via similar magmatic processes. Geochemical features such as the inverse correlations of Al_2O_3, Sr, and Eu/Gd with SiO_2 suggest that the ELM rocks evolved consistently through plagioclase-dominated fractionation from similar parental magmas. Because plagioclase is stable at pressures lower than 0.5–0.7 GPa in hydrous tholeiitic or andesitic magmas (i.e., potential parents of magmatic suites in volcanic arc environment; Green 1982), ELM magmas must have evolved in parental chambers at shallow crustal levels (i.e., <20 km depth).

The range of Pb and Sr isotopic values of ELM rocks indicates that different sources provided Pb and Sr to ELM magmas. The lead isotope spread of ELM rocks between the orogen and upper crust evolution curves (Fig. 4) suggests mixing between a low radiogenic lead source, isotopically compatible with a MORB-type mantle enriched by pelagic sediments (see above), and a high radiogenic end-member, isotopically compatible with compositions of the basement rocks of the Chaucha, Loja, and Tahuín terranes (Fig. 4) through which

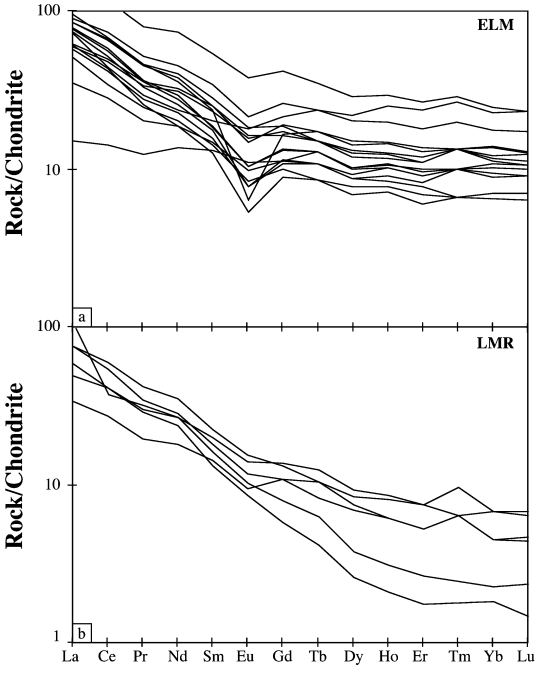

Fig. 8 REE spectra of magmatic rocks of the ELM and LMR groups

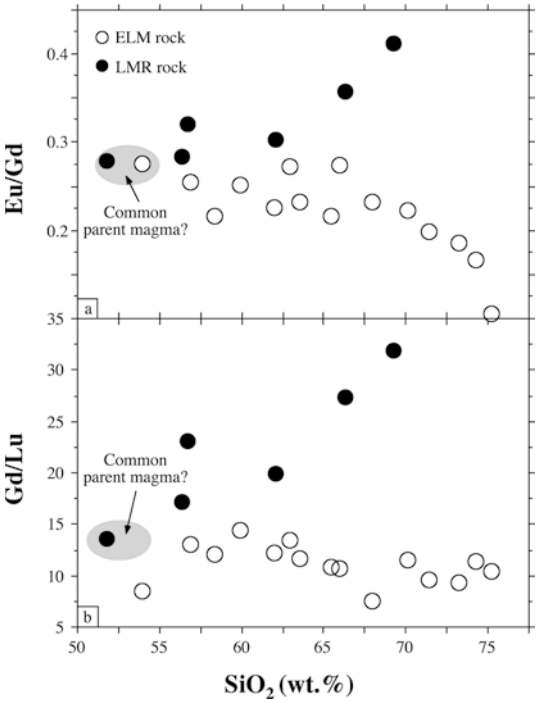

Fig. 9 Eu/Gd and Gd/Lu versus SiO_2 plots for the magmatic rocks investigated in this study

ELM magmas ascended (Figs. 1 and 3). Also, initial $^{87}Sr/^{86}Sr$ values of ELM rocks (0.7041–0.7058) are compatible with assimilation of radiogenic rocks of the Chaucha, Loja, and Tahuín terranes by mantle-derived magmas (Fig. 10). The moderate correlations of Sr and Pb isotope ratios with SiO_2, CaO, and Eu/Gd (Figs. 10 and 11) indicate that low radiogenic, mantle-derived, parent magmas of ELM rocks have assimilated radiogenic lithologies of the Chaucha, Loja, and Tahuín basements while undergoing plagioclase-dominated fractionation at shallow crustal levels (assimilation-fractional-crystallization, AFC process). A model of the AFC process yields a satisfactory approximation of the trends defined by the ELM rocks in Fig. 11.

In contrast, geochemical features of LMR rocks, such as increasing Eu/Gd with SiO_2 and the lack of Eu negative anomaly, suggest the absence of plagioclase fractionation in LMR magmas and indicate that the latter were formed/evolved at greater pressures than those of plagioclase stability, i.e., at depths greater than 20 km (Green 1982). The strong HREE depletions ($La/Yb = 49–69$, $Gd/Lu = 28–32$; Figs. 8 and 9) of some LMR rocks (samples E94021 and E99007) require the involvement of garnet as a residual phase in the source of LMR magmas. Indeed, the covariations of REE with isotope ratios in LMR rocks (Fig. 11) fit a model of mixing between a low radiogenic basic magma (A in Fig. 11) and a more felsic magma (B in Fig. 11) issued from the partial melting of a ^{87}Sr- and ^{207}Pb-rich, residual garnet-bearing ($Gd/Lu > 30$) rock. Overall, most of the LMR rocks have geochemical features of adakite-type magmas, notably high Sr/Y ratios (> 20), low Y (≤ 19 ppm), and low Yb (≤ 1.5 ppm) (Table 1; Fig. 12).

The signatures of LMR rocks could be interpreted to result from the interaction of a slab-derived melt (adakite, end-member B in Fig. 11) with the mantle wedge (end-member A in Fig. 11) as suggested for recent lavas of Ecuador (e.g., Samaniego et al. 2002). However, the LMR rocks investigated in the present study are unlikely to carry a significant slab melt component for at least two reasons. First, the negative Nb and Zr anomalies in the primitive mantle-normalized spectra of all investigated LMR rocks (Fig. 6) are of identical magnitude to those of the mantle-derived non-adakitic ELM rocks. If slab melts were involved in the formation of LMR rocks, the latter should be Nb- and Zr-enriched compared to ELM rocks (see also Samaniego et al. 2002). For instance, the melting experiments of Rapp et al. (1999) reveal that dacitic to rhyolitic slab melts should have Zr concentrations > 320 ppm whereas the most evolved dacitic to rhyolitic LMR rocks have Zr concentrations of only 130 ppm. Secondly, slab melting should result in a lead isotope shift of LMR rocks towards the isotopic field of the Galapagos and Marquesas rocks (Fig. 4) because during Mio-Pliocene times the flat subducting slabs, presumably undergoing melting, were the Carnegie ridge, derived from the Galapagos hotspot, under central and northern Ecuador (Gutscher et al. 1999b), and the Inca plateau, an inferred mirror of the Marquesas plateau (Gutscher et al. 1999a), under southern Ecuador (Fig. 4). Despite this, the LMR rocks have the same $^{206}Pb/^{204}Pb$ isotopic range as the non-adakitic ELM rocks and do not display any shift towards the compositions of Galapagos and Marquesas

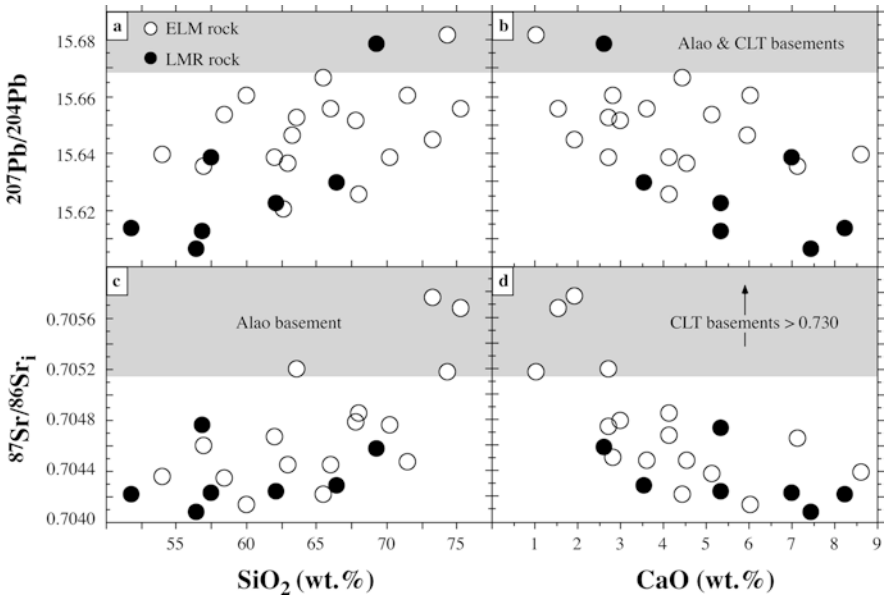

Fig. 10 Pb and Sr isotope compositions versus SiO_2 and CaO plots for the magmatic rocks investigated in this study

rocks, suggesting that neither the Inca plateau nor the Carnegie ridge were significantly involved in the genesis of LMR magmas (Fig. 4). Lead isotope data suggest that the ELM and LMR groups have the same source, i.e., the mantle wedge (Fig. 4). Also, in the lead versus strontium isotope space none of the LMR rocks has an isotopic composition compatible with melting of the Inca plateau or Carnegie ridge (Fig. 13). Indeed, their radiogenic Pb and Sr isotope compositions are incompatible even with melting of a MORB-type slab (Fig. 13).

Geochemistry of ELM/LMR magmatic rocks and geodynamic evolution

To explain the adakite-type signatures of LMR rocks we propose a model in which mantle-derived LMR magmas have ponded at depth, probably at the mantle-crust interface (the thickness of the crust is ~40–50 km in central-southern Ecuador: Feininger and Seguin 1983), where they partially melted and assimilated variable amounts of moderately radiogenic, residual garnet-bearing rocks and possibly evolved at the same time through plagioclase-free and amphibole fractionation in a process similar to MASH (melting-assimilation-storage-homogenization, Hildreth and Moorbath 1988). Similar models have been proposed to explain the adakite-like signatures of recent Central Andean and Ecuadorian magmas (Atherton and Petford 1993; Petford et al. 1996; Arculus et al. 1999; Richards et al. 2001; Kay and Mpodozis 2002; Kay and Kay 2002; Garrison and Davidson 2003).

The rocks partially melted and assimilated by the mantle-derived LMR magmas could include meta-basalts/andesites of the Jurassic Alao island arc terrane, which form a large portion of the exposed basement of LMR rocks and may have been underplated beneath the Ecuadorian crust during the Jurassic arc formation (Arculus et al. 1999). The range of lead and strontium isotopic compositions observed in the LMR magmas is compatible with assimilation of the Alao meta-basalts/andesites (Figs. 4 and 10). Additionally, these island arc meta-basalts/andesites have low contents of Nb (2.95 ± 1.4 ppm; N = 22: Litherland et al. 1994 plus our data in Table 1) and Zr (49.6 ± 16.4 ppm; N = 20: Litherland et al. 1994 plus our data in Table 1) compared to Pacific N-MORB ($Nb = 4.2 \pm 1.7$, N = 37; $Zr = 111.9 \pm 35.1$, N = 275: Geochemical Earth Reference Model: http://earthref.org/GERM/main.htm) and Pacific E-MORB ($Nb = 10.0 \pm 2.2$, N = 7; $Zr = 174.9 \pm 65.9$, N = 48: Geochemical Earth Reference Model: http://earthref.org/GERM/main.htm). Therefore, their partial melting is also compatible with the low contents of Nb and Zr in LMR magmas (see above), different from that expected from partial melting of subducted Pacific N-MORB or E-MORB-type (i.e., Carnegie ridge, Inca plateau) oceanic crusts (see above).

The distinct geochemical signatures of the ELM and LMR magmas may be the outcome of the changing geotectonic regime on the overriding Ecuadorian continent during Tertiary (see above and Fig. 14). ELM rocks (~50–9 Ma) were formed during a period of dominant transpression ± extension (Noblet et al. 1996; Hungerbühler et al. 2002) and were emplaced in a crustal domain characterized by the presence of trench-parallel and trench-normal faults and sutures (Figs. 1 and 3). The combination of these factors might have allowed a relatively continuous passive ascent of magmas to shallow crustal levels along trench-normal structures of the Huancabamba deflection or in dilational jogs along trench-parallel structures during the period ~50–9 Ma (Fig. 14; see also Corbett and Leach 1998, Tosdal and Richards 2001 for similar models).

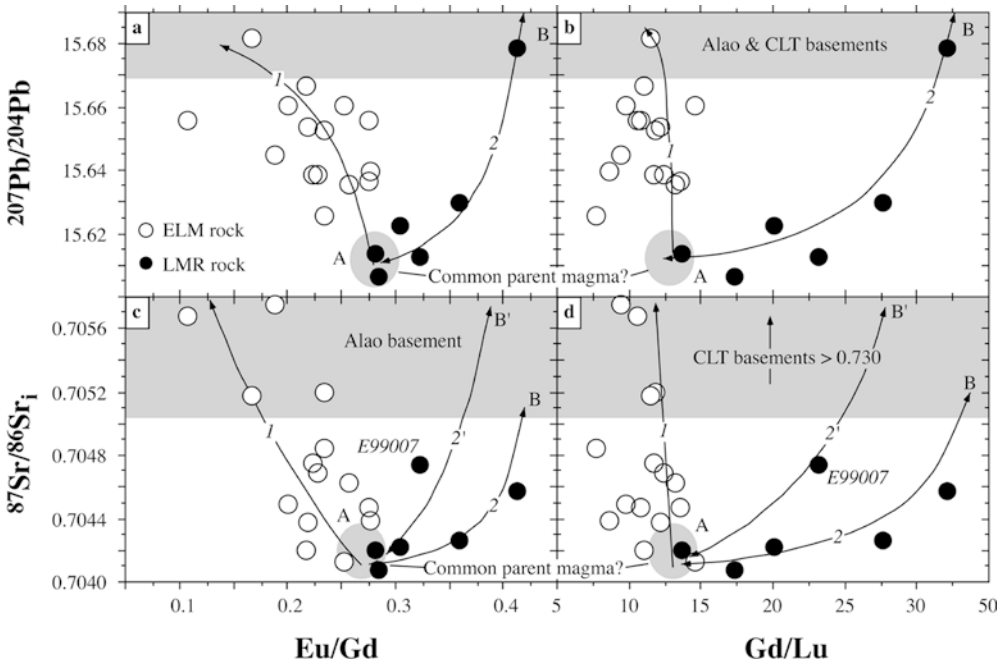

Fig. 11 Pb and Sr isotope compositions versus Eu/Gd and Gd/Lu plots for the magmatic rocks investigated in this study. *Path 1* represents a modeled AFC trend for a magma (A) with initial REE and isotopic compositions corresponding to those of a mantle-derived basic magma that is crystallizing 35 wt% plagioclase, 45 wt% clinopyroxene, and 20 wt% olivine and assimilating radiogenic metamorphic rocks of the Ecuadorian basement. The end point (*arrow tip*) of *path 1* corresponds to 75% crystallization of the initial magma. *Path 2* represents mixing between the mantle-derived basic magma A and a magma (B) issued from a 35% melting of a rock consisting of 75 wt% clinopyroxene and 25 wt% garnet and having Pb and Sr isotope compositions of the Alao meta-basalts/andesites ($^{207}Pb/^{204}Pb = 15.70$; $^{87}Sr/^{86}Sr = 0.7051$). The position of sample E99007 can be explained by mixing (*path 2'*) of magma A and magma B'. The latter has the same origin as magma B but has a more radiogenic composition ($^{87}Sr/^{86}Sr = 0.7090$). The position of sample E99007 might be due to a larger variability of Sr isotope compositions of the Alao meta-basalts/andesites than that measured in the two samples analyzed (Table 1). In contrast, the reduced scatter in the trends of Figs. 9a and b is probably related to the homogeneous $^{207}Pb/^{204}Pb$ isotope compositions of the Alao meta-basalts/andesites (Table 1). The modeled trends have been calculated using the equations of DePaolo (1981). *CLT* Chaucha-Loja-Tahuín

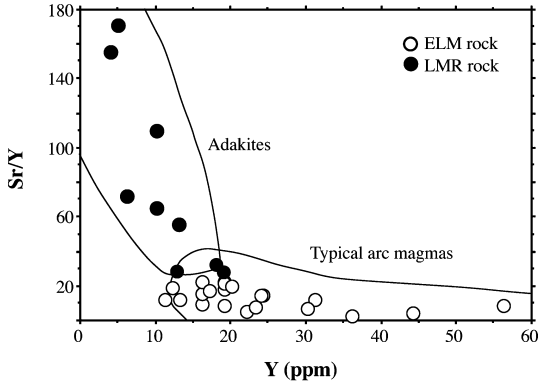

Fig. 12 Sr/Y versus Y diagram for the ELM and LMR rocks. Fields of adakites and typical arc magmas are based on Defant and Drummond (1993), Maury et al. (1996), and Sajona and Maury (1998)

LMR rocks (~8–0 Ma) were formed during a period of dominant tectonic compression (from 9 Ma to present: Noblet et al. 1996; Steinmann et al. 1999; Hungerbüher et al. 2002), probably following the subduction of the Carnegie ridge (~8–10 Ma ago), and in a crustal domain characterized by the presence only of trench-parallel structures (Fig. 1 and 3). During compression, trench-parallel structures are sealed and magmas are impeded to rise by buoyancy (e.g., Corbett and Leach 1998; Tosdal and Richards 2001). Under these conditions LMR magmas could have ponded and evolved at lower crustal or subcrustal levels (at depths possibly > 40–50 km: Fig. 14), yielding the adakite-type signatures discussed above.

Metallogenic implications

Recent studies (e.g., Thiéblemont et al. 1997; Kay et al. 1999; Richards et al. 2001; Oyarzun et al. 2001) have highlighted a link between several large porphyry-Cu/epithermal mineralization and magmatic rocks with adakite-type signatures, independently from the genetic interpretation of the adakite-type rocks as resulting from the interaction of mantle-derived magmas with the lower crust (Kay et al. 1999; Richards et al. 2001; Richards 2002; Rabbia et al. 2002) or from slab melting (Sajona and Maury 1998; Oyarzun et al. 2001; Oyarzun et al. 2002).

Our study shows that the great majority of the known Tertiary porphyry-Cu and epithermal deposits of Ecuador, which are relatively small (≤ 165 Mt: Table 2), are spatially and temporally associated with non-adakitic, calc-alkaline ELM-type magmatic rocks.

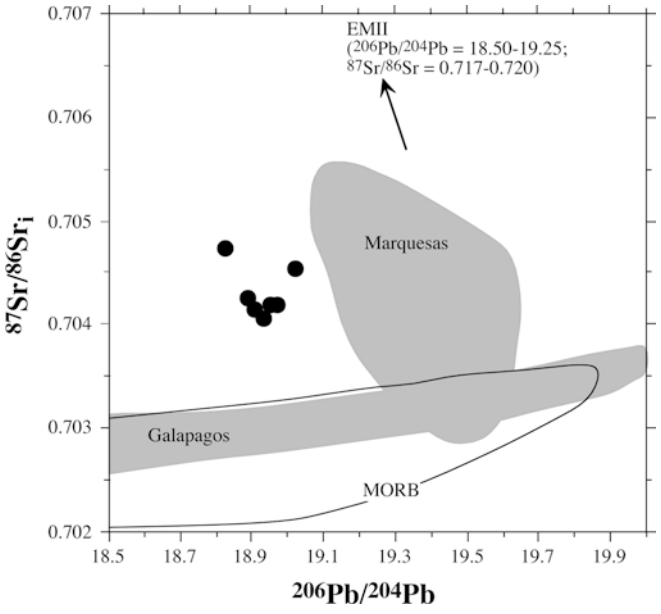

Fig. 13 $^{87}Sr/^{86}Sr_i$ versus $^{206}Pb/^{204}Pb$ plot of the LMR rocks investigated in the present study. Compositional fields of the Galapagos and Marquesas rocks as well as MORB are from Zindler and Hart (1986). *EMII* is the Enriched Mantle II component of Zindler and Hart (1986) representing a mantle enriched by pelagic sediments. Isotopic compositions of the LMR rocks may result from mixing of MORB and EMII

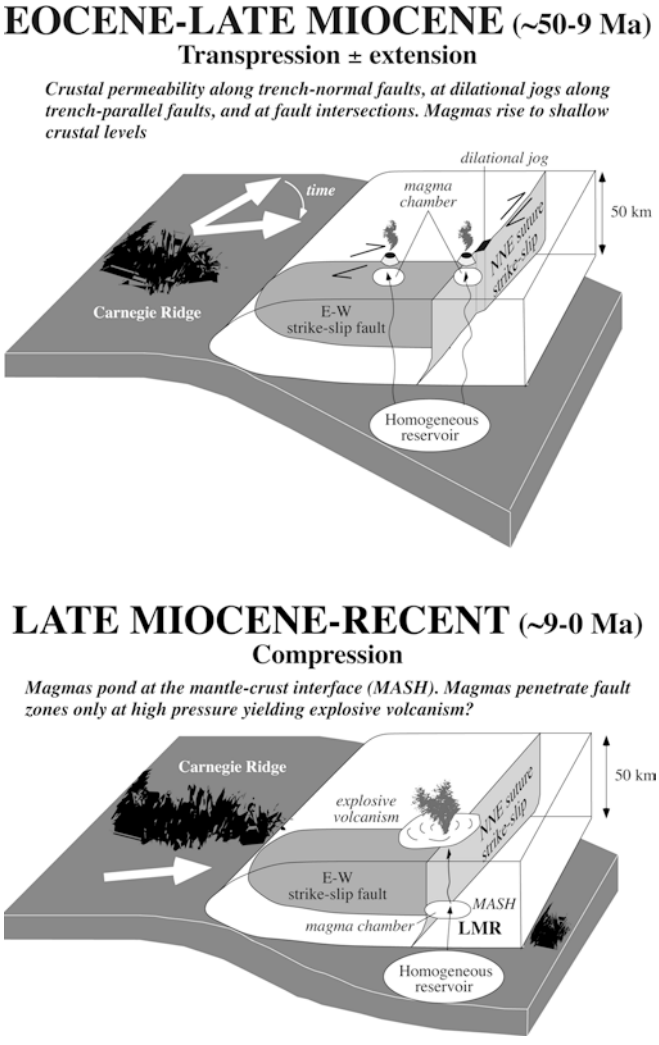

Fig. 14 Cartoon showing the geodynamic control on the geochemical evolution of Ecuador magmas from the ELM- to the LMR-type at the end of Miocene. ELM magmas were formed during a period of dominant transpression ± extension (~50–9 Ma). Mantle-derived magmas could rise at shallow crustal levels through trench-normal structures or at dilational jogs along trench-parallel structures. LMR magmas were forced to pond at depth, possibly at the mantle-crust interface, during a dominant compression phase started ~9 Ma ago with the subduction of the aseismic Carnegie ridge (Spikings et al. 2001; Hungerbühler et al. 2002)

These rocks originated from mantle-derived magmas that have evolved through plagioclase-dominated fractionation and assimilation of Pb- and Sr-radiogenic basement rocks in parental magma chambers situated at shallow crustal levels (< 20 km depth) during a prolonged period of dominant transpression ± extension. Since evolution of parental magmas at shallow crustal levels is an essential step in the process conducive to porphyry-Cu and related deposits (Tosdal and Richards 2001) the fertility of ELM magmatism is not surprising. Nevertheless, additional magmatic factors are probably required to form large porphyry-Cu and epithermal deposits as perhaps suggested by the association of several major porphyry-Cu and epithermal deposits with magmas having peculiar geochemical features, e.g., those of adakite-type magmas (see above).

In contrast with the ELM rocks, Late Miocene-Recent (LMR) magmatic rocks of Ecuador have geochemical signatures of adakite-type magmas and were formed during a period of dominant compression. Trace and rare earth elements as well as lead and strontium isotopes suggest that the adakite-type signatures of LMR rocks are due to MASH-type processes and not to slab melting. Based on comparisons with the geochemistry of magmatic rocks associated with major porphyry-Cu/epithermal deposits at convergent margins (see above), LMR rocks are potentially fertile. Despite this, only the high sulfidation epithermal deposit of Quimsacocha is associated with LMR magmatic rocks. To explain the apparent low fertility of LMR rocks we propose two divergent hypotheses that are equally plausible on the basis of geological constraints and formation processes of porphyry-Cu/epithermal deposits.

The paucity of porphyry-Cu/epithermal deposits associated with LMR magmatism might simply result from exposure level. Thick recent volcanic deposits extensively cover central and northern Ecuador (Fig. 3), where the majority of LMR rocks occur. In contrast such a recent cover is absent in southern Ecuador (Fig. 3), where ELM magmatism occurs, due to the lack of recent volcanism in this part of the country. Therefore, porphyry-Cu/epithermal mineralization associated with LMR magmatism might be simply concealed under the recent volcanic cover.

An alternative scenario is that extensive porphyry-Cu/epithermal mineralization has not formed in association with LMR rocks. Tosdal and Richards (2001) point out that at orthogonal convergent margins, where major trench-parallel fault zones are compressed (as is the case for Ecuador at the time of LMR magmatism), magmas will pond at the base of the lithosphere and will evolve through MASH processes (as it occurs for LMR rocks according to our data). Under these conditions, ascent to the surface may be restricted to overpressured magmas that would erupt violently without significant residence in upper crustal magma chambers (Fig. 14). This scenario is unfavorable for porphyry-Cu/epithermal mineralization (Tosdal and Richards 2001). The LMR magmatism of Ecuador might represent this stage because it is associated with a period of dominant compression and has been mostly of the explosive type since ~9 Ma (Fig. 14). More work is clearly needed to understand the metallogenic potential of the LMR magmatism.

Conclusions

The large majority of known porphyry-Cu and epithermal deposits of Ecuador are spatially and chronologically associated with magmatic rocks of Eocene to Late Miocene age (ELM, ~50–9 Ma). The ELM magmatic rocks originated from mantle-derived calc-alkaline magmas that have evolved in parental chambers at shallow crustal levels (< 20 km) through plagioclase-dominated fractionation. These magmas were emplaced at shallow crustal levels during a prolonged period of transpression ± extension in the Ecuadorian continental crust.

Only the ~5 Ma old Quimsacocha epithermal deposit has been recognized so far in association with Late Miocene to Recent (LMR) magmatic rocks. The LMR rocks investigated in this study have adakite-type features that are interpreted to result not from slab-melting but from the evolution of mantle-derived magmas in parental chambers situated at subcrustal levels during a prolonged compressional phase initiated ~9 Ma ago. At these depths, mantle-derived magmas assimilated residual garnet-bearing rocks (possibly underplated metabasalts of the Jurassic Alao arc) and evolved through plagioclase-free and amphibole fractionation (MASH-type processes). LMR magmatic rocks of Ecuador bear geochemical similarities with the magmatic rocks associated with large porphyry-Cu/epithermal deposits of the Central Andes and of other magmatic arcs (e.g., Philippines). However, in Ecuador, despite the metallogenic potential of LMR rocks, only one deposit (Quimsacocha) is associated with LMR-type magmatism. More work is needed to understand whether the apparent low mineralization associated with LMR magmatic rocks is real or is simply due to exposure level.

Acknowledgements We thank Jeremy Richards (University of Alberta, Edmonton, Canada), Bruce Rohrlach (Australian National University, Canberra, Australia), Thomas Bissig (University of British Columbia, Vancouver, Canada), and Bernd Lehmann (University of Clausthal, Germany) for their careful reviews that have improved a previous version of this work. We are also grateful to Jan Kramers (University of Bern, Switzerland) and Ronny Schoenberg (University of Hannover, Germany) for the collaboration in the Re-Os analyses, to Holly Stein (AIRIE Group, Colorado State University, Fort Collins, Colorado) for supplying an aliquot of HLP-5 molybdenite sample, to Michael Dungan (University of Geneva, Switzerland) for stimulating comments, as well as to Agustín Paladines (Universidad Central, Quito, Ecuador) and to Jaime Jarrín (Ministerio de Energía y Minas, Quito, Ecuador) for assistance during sample collection. This study was funded by the Swiss National Foundation (grant # 2000–054150).

References

Arculus RJ, Lapierre H, Jaillard E (1999) Geochemical window into subduction and accretion processes: Raspas metamorphic complex, Ecuador. Geology 27:547–550

Aspden JA, Litherland M (1992) The geology and Mesozoic collisional history of the Cordillera Real, Ecuador. Tectonophysics 205:187–204

Atherton MP, Petford N (1993) Generation of sodium-rich magmas from newly underplated basaltic crust. Nature 362:144–146

Barreiro BA, Clark AH (1984) Lead isotopic evidence for evolutionary changes in magma-crust interaction, Central Andes, southern Peru. Earth Planet Sci Lett 69:30–42

Beate B, Monzier M, Spikings R, Cotton J, Silva J, Bourdon E, Eissen J-P (2001) Mio-Pliocene adakite generation related to flat subduction in southern Ecuador: the Quimasacocha volcanic center. Earth Planet Sci Lett 192:561–570

BGS and CODIGEM (1999) Mapa Geologico de la Cordillera Occidental del Ecuador. Mision Britanica, CODIGEM, Quito, Ecuador

Bristow CR, Hoffstetter R (1977) Lexique stratigraphique international: Ecuador, vol 5, 2. CNRS, Paris

Castillo PR, Janney PE, Solidum RU (1999) Petrology and geochemistry of Camiguin Island, southern Philippnes: insights to the source of adakites and other lavas in a complex arc setting. Contrib Mineral Petrol 134:33-51

Chiaradia M, Fontboté L (1999) Preliminary new lead isotope data on ores and rocks of Ecuador: assessing metal sources in a complex subduction-related environment. In: Stanley CJ et al. (eds) Mineral deposits: processes to processing. Balkema, Rotterdam, pp 1315–1318

Chiaradia M, Fontboté L (2001) Radiogenic lead signatures in Au-rich VHMS ores and associated volcanic rocks of the Early Tertiary Macuchi island arc (Western Cordillera of Ecuador). Econ Geol 96:1361–1378

Chiaradia M, Fontboté L. (2002) Lead isotope systematics of Late Cretaceous-Tertiary Andean arc magmas and associated ores between 8°N and 40°S: evidence for latitudinal mantle heterogeneity beneath the Andes. Terra Nova 14:337–342

Chiaradia M, Fontboté L. (2003) Separate lead isotope analyses of leachate and residue rock fractions: implications for metal source tracing. Mineral Deposita 38:185–195

Chiaradia M, Fontboté L, Paladines A (2003) Lead isotope compositions of mineral deposits and crustal rocks of Ecuador (1°N-4°S): evidence for a multi-terrane composite crust. Econ Geol (submitted)

Corbett GJ, Leach TM (1998) Structure of magmatic ore systems. In: Corbett GJ, Leach TM, Southwest Pacific rim gold-copper systems: structure, alteration, and mineralization. Society of Economic Geologists Special Publication 6:31–67

Daly MC (1989) Correlation between Nazca/Farallon plate kinematics and forearc basin evolution in Ecuador. Tectonics 8:769–790

Defant MJ, Drummond MS (1990) Derivation of some modern arc magmas by melting of young subducted lithosphere. Nature 347:662–665

Defant MJ, Drummond MS (1993) Mount St. Helens: potential example of the partial melting of the subducted lithosphere in volcanic rocks. Geology 21:547–550

DePaolo DJ (1981) Trace element and isotopic effects of combined wall-rock assimilation and fractional crystallization. Earth Planet Sci Lett 53:189–202

Drummond MS, Defant MJ, Kepezhinskas PK (1996) Petrogenesis of slab-derived trondhjemite-tonalite-dacite/adakite magmas. In: M Brown et al. (eds) The third Hutton symposium on the origin of granites and related rocks. Geological Society of America Special Paper 315:205–215

Feininger T (1987) Allochthonous terranes in the Andes of Ecuador and northwestern Peru. Can J Earth Sci 24:266–278

Feininger T, Seguin MK (1983) Simple Bouguer gravity anomaly field and the inferred crustal structure of continental Ecuador. Geology 11:40–44

Francis PW, Moorbath S, Thorpe RS (1977) Strontium isotope data for recent andesites in Ecuador and North Chile. Earth Planet Sci Lett 37:197–202

Garrison JM, Davidson JP (2003) Dubious case for slab melting in the Northern volcanic zone of the Andes. Geology 31:565–568

Goossens PJ (1972) Metallogeny in Ecuadorian Andes. Econ Geol 67:458–468

Goossens PJ, Hollister VF (1973) Structural control and hydrothermal alteration pattern at Chaucha porphyry copper, Ecuador. Mineral Deposita 8:321–331

Green TH (1982) Anatexis of mafic crust and high pressure crystallization of andesites. In: Thorpe RS (ed) Andesites. Wiley, New York , pp 465–487

Gutscher M-A, Malavieille J, Lallemand S, Collot J-Y (1999b) Tectonic segmentation of the North Andean margin: impact of the Carnegie Ridge collision. Earth Planet Sci Lett 168:255–270

Gutscher M-A, Olivet J-L, Aslanian D, Eissen J-P, Maury R (1999a) The ''lost Inca Plateau'': cause of flat subduction beneath Peru? Earth Planet Sci Lett 171:335–341

Harmon RS, Thorpe RS, Francis PW (1981) Petrogenesis of Andean andesites from combined O-Sr isotope relationships. Nature 290:396

Hawkesworth CJ, Norry MJ, Roddick JC, Baker E, Francis PW, Thorpe RS (1979) $^{143}Nd/^{144}Nd$, $^{87}Sr/^{86}Sr$, and incompatible element variations in calc-alkaline andesites and plateau lavas from South America. Earth Planet Sci Lett 42:45–57

Hey R (1977) Tectonic evolution of the Cocos-Nazca spreading center. Bull Geol Soc America 88:1404–1420

Hildreth W, Moorbath S (1988) Crustal contributions to arc magmatism in the Andes of central Chile. Contrib Mineral Petrol 98:455–489

Hughes RA, Pilatasig LF (2002) Cretaceous and Tertiary terrane accretion in the Cordillera Occidental of the Andes of Ecuador. Tectonophysics 345:29–48

Hungerbühler D, Steinmann M, Winkler W, Seward D, Egüez A, Peterson DE, Helg U, Hammer C (2002) Neogene stratigraphy and Andean geodynamics of southern Ecuador. Earth Sci Rev 57:75–124

Jaillard E, Benítez S, Mascle GH (1997) Les deformations paléogènes de la zone d'avant-arc sud-équatorienne en relation avec l'évolution géodynamique. Bull Soc Géol France 4:403–412

Jaillard E, Soler P (1996) Cretaceous to early Paleogene tectonic evolution of the northern Central Andes (0–18°) and its relations to geodynamics. Tectonophysics 259:41–53

Kay RW, Kay SM (2002) Andean adakites: three ways to make them. Acta Petrol Sinica 18:303–311

Kay SM, Mpodozis C (2002) Magmatism as a probe to the Neogene shallowing of the Nazca plate beneath the modern Chilean flat-slab. J South Amer Earth Sci 15:39–57

Kay SM, Mpodozis C, Coira B (1999) Neogene magmatism, tectonism, and mineral deposits of the Central Andes (22° to 33°S latitude). In: Skinner BJ (ed) Geology and ore deposits of the Central Andes. Society of Economic Geologists, Special Publication 7:27–59

Kennerley JB (1980) Outline of the geology of Ecuador. Institute of Geological Sciences: Overseas Geology and Mineral Resources 58:17

Lavenu A, Noblet C, Bonhomme MG, Egüez A, Dugas F, Vivier G (1992) New K-Ar age dates of Neogene and Quaternary volcanic rocks from the Ecuadorian Andes: implications for the relationship between sedimentation, volcanism, and tectonics. J South Amer Earth Sci 5, 309–320

LeBas MJ, Le Maitre RW, Streckeisen A, Zanettin B (1986) A chemical classification of volcanic rocks based on the total alkali-silica diagram. J Petrol 27:745–750

Litherland M, Aspden JA (1992) Terrane-boundary reactivation: a control on the evolution of the Northern Andes. J South Amer Earth Sci 5:71–76

Litherland M, Aspden JA, Jemielita RA (1994) The metamorphic belts of Ecuador. Overseas Memoir 11. BGS, Keyworth

Mamberti M, Lapierre H, Bosch D, Jaillard E, Ethien R, Hernandez J, Polvé M (2003) Accreted fragments of the Late Cretaceous Caribbean–Colombian Plateau in Ecuador. Lithos 66:173–199

Markey R, Stein H, Morgan J (1998) Highly precise Re-Os dating for molybdenite using alkaline fusion and NTIMS. Talanta 45:935–946

Maury RC, Sajona FG, Pubellier M, Bellon H, Defant MJ (1996) Fusion de croûte océanique dans les zones de subduction/collision récentes: l'exemple de Mindanao (Philippines). Bull Soc Géol Fr 167:579–595

Mourier T, Laj C, Mégard F, Roperch P, Mitouard P, Farfan Medrano A (1988) An accreted continental terrane in northwestern Peru. Earth Planet Sci Lett 88:182–192

Mungall JE (2002) Roasting the mantle: slab melting and the genesis of major Au and Au-rich Cu deposits. Geology 30:915–918

Nägler TF, Frei R (1997) 'Plug in' Os distillation. Schweiz Mineral Petrogr Mitt 77:123–127

Noblet C, Lavenu A, Marocco R (1996) Concept of continuum as opposed to periodic tectonism in the Andes. Tectonophysics 255:65–78

Oyarzun R, Márquez A, Lillo J, López I, Rivera S (2001) Giant versus small porphyry copper deposits of Cenozoic age in northern Chile: adakitic versus normal calc-alkaline magmatism. Mineral Deposita 36:794–798

Oyarzun R, Márquez A, Lillo J, López I, Rivera S (2002) Reply to discussion on ''Giant versus small porphyry copper deposits of Cenozoic age in northern Chile: adakitic versus normal calc-alkaline magmatism'' by Oyarzun R, Márquez A, Lillo J, López I, Rivera S (Mineral Deposita 36:794–798, 2001). Mineral Deposita 37:795–799

Pearce JA (1983) Role of sub-continental lithosphere in magma genesis at active continental margins. In CJ Hawkesworth, MJ Norry (eds) Continental basalts and mantle xenoliths. Shiva Geology Series, Cheshire UK, 230–249

Petford N, Atherton MP, Halliday AN (1996) Rapid magma production rates, underplating and remelting in the Andes: isotopic evidence from northern-central Peru (9–11°S). J South Amer Earth Sci 9:69–78

Pratt WT, Figueroa JF, Flores BG (1997) Geology of the Cordillera Occidental of Ecuador between 3°00' and 4°00'S. Proyecto de Desarrollo Minero y Control Ambiental (PRODEMINCA), Programa de Información Cartográfica y Geologia (PICG) CODIGEM-BGS, Report no 1

Prodeminca (2000a) Evaluacion de distritos mineros del Ecuador, vol 2—Depositos epitermales en la Cordillera Andina. UCP Prodeminca Proyecto MEM BIRF 36–55 EC, Quito, Ecuador

Prodeminca (2000b) Evaluacion de distritos mineros del Ecuador, vol 4—Depositos porfidicos y epi-mesotermales relacionados con intrusiones de las Cordilleras Occiental y Real. UCP Prodeminca Proyecto MEM BIRF 36–55 EC, Quito, Ecuador

Rabbia OM, Hernández LB, King RW, López-Escobar L (2002) Discussion on ''Giant versus small porphyry copper deposits of Cenozoic age in northern Chile: adakitic versus normal calc.alkaline magmatism'' by Oyarzun et al. (Mineral Deposita 36:794–798, 2001). Mineral Deposita 37:791–794

Rapp RP, Shimizu N, Norman MD, Applegate GS (1999) Reaction between slab-derived melts and peridotite in the mantle wedge: experimental constraints at 3.8 GPa. Chem Geol 160:335–356

Richards JP (2002) Discussion on "Giant versus small porphyry copper deposits of Cenozoic age in northern Chile: adakitic versus normal calc-alkaline magmatism" by Oyarzun et al. (Mineral Deposita 36:794–798, 2001). Mineral Deposita 37:788–790.

Richards JP, Boyce AJ, Pringle MS (2001) Geologic evolution of the Escondida area, northern Chile: A model for spatial and temporal localization of porphyry Cu mineralization. Econ Geol 96:271–305

Reynaud C, Jaillard E, Lapierre H, Mamberti M, Mascle GH (1999) Oceanic plateau and island arcs of southwestern Ecuador: their place in the geodynamic evolution of northwestern South America. Tectonophysics 307:235-254

Roy-Barman M, Allègre CJ (1995) $^{187}Os/^{186}Os$ in oceanic island basalts: tracing oceanic crust recycling in the mantle. Earth Planet Sci Lett 129:145–161

Sajona FG, Maury R (1998) Association of adakites with gold and copper mineralization in the Philippines. Comptes Rendus Acad Sci Paris 326:27–34

Samaniego P, Martin H, Robin C, Monzier M (2002) Transition from calc-alkalic to adakitic magmatism at Cayambe volcano, Ecuador: insights into slab melts and mantle wedge interactions. Geology 30:967–970

Schoenberg R, Nägler TF, Kramers JD (2000) Precise Os isotope ratio and Re-Os isotope dilution measurements down to the picogram level using multicollector inductively coupled plasma mass spectrometry. Internat J Mass Spectrom 197:85–94

Sillitoe RH (2000) Gold-rich porphyry deposits: descriptive and genetic models and their role in exploration and discovery. Rev Econ Geol 13:315–344

Spencer RM, Montenegro JL, Gaibor A, Perez EP, Mantilla G, Viera F, Spencer CE (2002) The Portovelo-Zaruma mining camp, SW Ecuador: porphyry and epithermal environments. SEG Newsletter 49:(1)8–14

Spikings RA, Winkler W, Seward D, Handler R (2001) Along-strike variations in the thermal and tectonic response of the continental Ecuadorian Andes to the collision with heterogeneous oceanic crust. Earth Planet Sci Lett 186:57–73

Steinmann M, Hungerbühler D, Seward D, Winkler W (1999) Neogene tectonic evolution and exhumation of the southern Ecuadorian Andes: a combined stratigraphy and fission-track approach. Tectonophysics 307:255–276

Sun SS, McDonough WF (1989) Chemical and isotopic systematics of oceanic basalts: Implications or mantle composition and processes. In: Saunders AD, Norry MJ (eds) Magmatism in the ocean basins. Geological Society, London, Special Publication 42:313–346

Thiéblemont D, Stein G, Lescuyer JL (1997) Gisements épithermaux et porphyriques: la connection adakite. Comptes Rendus Acad Sci Paris 325:103–109

Tosdal RM, Richards JP (2001) Magmatic and structural controls on the development of porphyry $Cu \pm Mo \pm Au$ deposits. Rev Econ Geol 14:157–181

van Thournout F, Hertogen J, Quevado L (1992) Allochthonous terranes in northwestern Ecuador. Tectonophysics 205:205–221

van Thournout F, Salemink J, Valenzuela G, Merlyn M, Boven A, Muchez P (1996) Portovelo: A volcanic-hosted epithermal vein-system in Ecuador, South America. Mineral Deposita 31:269–276

Walker RJ (1988) Low-blank chemical separation of rhenium and osmium from gram quantities of silicate rock for measurement by resonance ionization mass spectrometry. Anal Chem 60:1231–1234

Zartman RE, Doe BR (1981) Plumbotectonics—the model. Tectonophysics 75:135–162

Zindler A, Hart S (1986) Chemical geodynamics. Ann Rev Earth Planet Sci 14:493–571